Quaternary Research (2025), 1–21
doi:10.1017/qua.2025.17

Research Article

Linking the tephrostratigraphy of the Pleistocene Naibadad Beds across the Laetoli area, Olduvai basin, and Ngorongoro volcano (Tanzania) using geochronology and tephra composition

Lindsay J. McHenry[a], Alan L. Deino[b], Terry Harrison[c]

[a]Department of Geosciences, University of Wisconsin-Milwaukee, 3209 N. Maryland Ave., Milwaukee, WI 53211, USA; [b]Berkeley Geochronology Center, 2455 Ridge Rd., Berkeley, CA 94709, USA and [c]Center for the Study of Human Origins, Department of Anthropology, New York University, New York, NY 10003, USA

Abstract

While geological and paleoanthropological studies at Laetoli have focused on the relatively fossiliferous Ndolanya and Laetolil beds, Laetoli's younger Naibadad and Olpiro beds provide an important record of Pleistocene volcanism, tectonics, and landscape evolution in northern Tanzania. This study documents the mineralogical and geochemical compositions of their tephra using EPMA of glass and phenocrysts, and their ages using $^{40}Ar/^{39}Ar$ geochronology. Naibadad Beds tephra is rhyolitic or trachytic, compositionally distinct from the underlying Ndolanya and overlying Olpiro beds in their mineral assemblages and glass and phenocryst compositions. The Naibadad Beds can be divided into chronostratigraphic clusters as follows: Lower (2.189–2.154 Ma), Middle (2.115–2.104 Ma), and Upper (2.036–2.004 Ma). Most Naibadad Beds tephra could not be compositionally differentiated, although the basal Naibadad Beds tuff is unique in having both trachytic glass and andradite garnet. The uppermost Naibadad Beds tuff at Locality 23 has rhyolitic glass and aenigmatite like Olduvai Gorge's Naabi ignimbrite and a similar age (2.033 Ma and 2.004 Ma, respectively), although they differ in feldspar and augite composition and are likely not from the same eruption. The lack of direct correlatives between Olduvai and Laetoli, which both derived tephra from Ngorongoro over the same time interval, is likely explained by paleotopography.

Keywords: Pleistocene; tephra; tephrostratigraphy; $^{40}Ar/^{39}Ar$; Laetoli

Introduction

Laetoli, most famous for its exquisitely preserved hominin footprints in tuffs from the Pliocene Laetolil Beds, preserves detailed paleoanthropological, paleoecological, sedimentological, and volcanic records stretching from > 4.4 Ma to the present (Leakey and Harris, 1987; Harrison, 2011a, 2011b; overview in Harrison et al., 2022). About 35 km southwest of Olduvai Gorge, Laetoli provides an earlier record of hominin activity, albeit with potential overlap to Olduvai in the youngest Laetoli strata. The potential for overlap has recently been expanded, given the discovery of older strata beneath surface exposures at Olduvai revealed through geological coring conducted by the Olduvai Gorge Coring Project (OGCP; Njau et al., 2021). Tephra preserved at Laetoli and Olduvai provide a record of volcanic activity from the nearby Ngorongoro Volcanic Highlands (Figure 1). These tephra provide an opportunity to establish a tephrostratigraphy linking basins and paleoanthropological sites.

The stratigraphy of the Laetoli area (Figure 2) includes the Lower Laetolil Beds (> 4.36–3.85 Ma), Upper Laetolil Beds (3.85–3.63 Ma), Lower Ndolanya Beds (3.58 Ma), Upper Ndolanya Beds (2.66 Ma), Naibadad Beds (2.155–2.057 Ma), Olpiro Beds (< 2.057 Ma), and Ngaloba Beds, as described by Hay (1987) and as dated by Drake and Curtis (1987) and Deino (2011). These strata are exposed by badlands-style erosion and correlated using sedimentology and tephrostratigraphy (e.g., Hay, 1987; Ditchfield and Harrison, 2011; Harrison and Kweka, 2011). The Laetolil Beds are the most extensively exposed and distributed (Figure 2), while the younger strata (Naibadad and Olpiro beds) are unevenly distributed, often filling erosional surfaces cut into the older strata.

Laetoli is renowned for discoveries within the Laetolil Beds, which host hominin trackways and have yielded a high diversity of fauna, including *Australopithecus afarensis* (Leakey, 1987a, b; Harrison, 2011c, d; Masao et al., 2016). The younger strata, however, also host an intriguing fossil and archaeological record (e.g., Ndessokia, 1990; Harrison, 2011c; Harrison et al., 2022). The Naibadad and Olpiro beds yield only a sparse fauna, the latter of which is associated with Oldowan tools (Ndessokia, 1990). The Lower Ngaloba Beds, biostratigraphically correlated to ca. 1.7–1.2 Ma, have produced faunal remains in association with Acheulian tools (Harris and Harris, 1981; Leakey, 1987c; Harrison and Kweka, 2011; Arenson et al., 2022). The Upper Ngolaba Beds, dated to > 200 ka (Manega, 1993), have yielded a fauna associated with an archaic *Homo sapiens* cranium and Middle Stone Age lithic

Corresponding author: Lindsay J. McHenry; Email: lmchenry@uwm.edu
Cite this article: McHenry, L.J., Deino, A.L., Harrison, T., 2025. Linking the tephrostratigraphy of the Pleistocene Naibadad Beds across the Laetoli area, Olduvai basin, and Ngorongoro volcano (Tanzania) using geochronology and tephra composition. *Quaternary Research*, 1–21. https://doi.org/10.1017/qua.2025.17

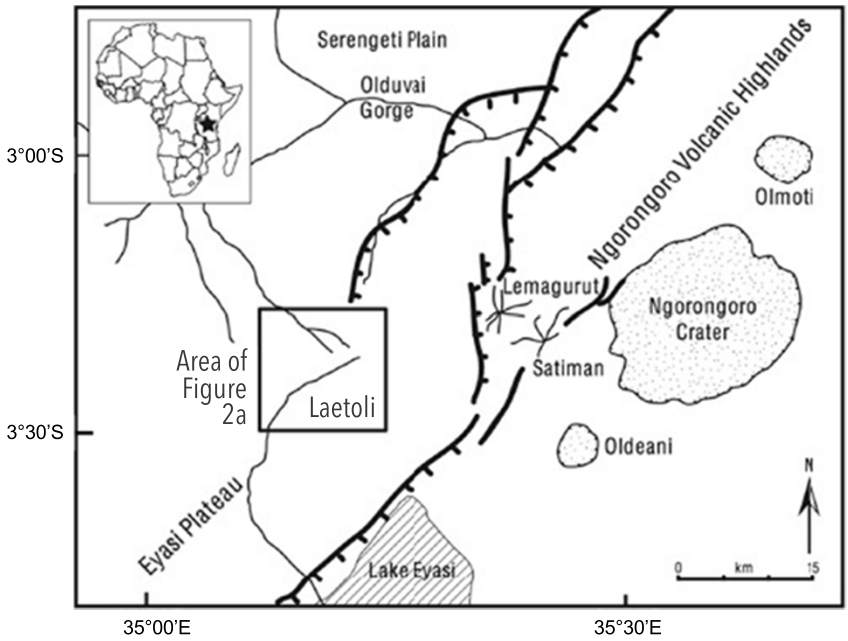

Figure 1. Regional map, showing location of Laetoli relative to Olduvai Gorge and volcanoes of the Ngorongoro Volcanic Highlands.

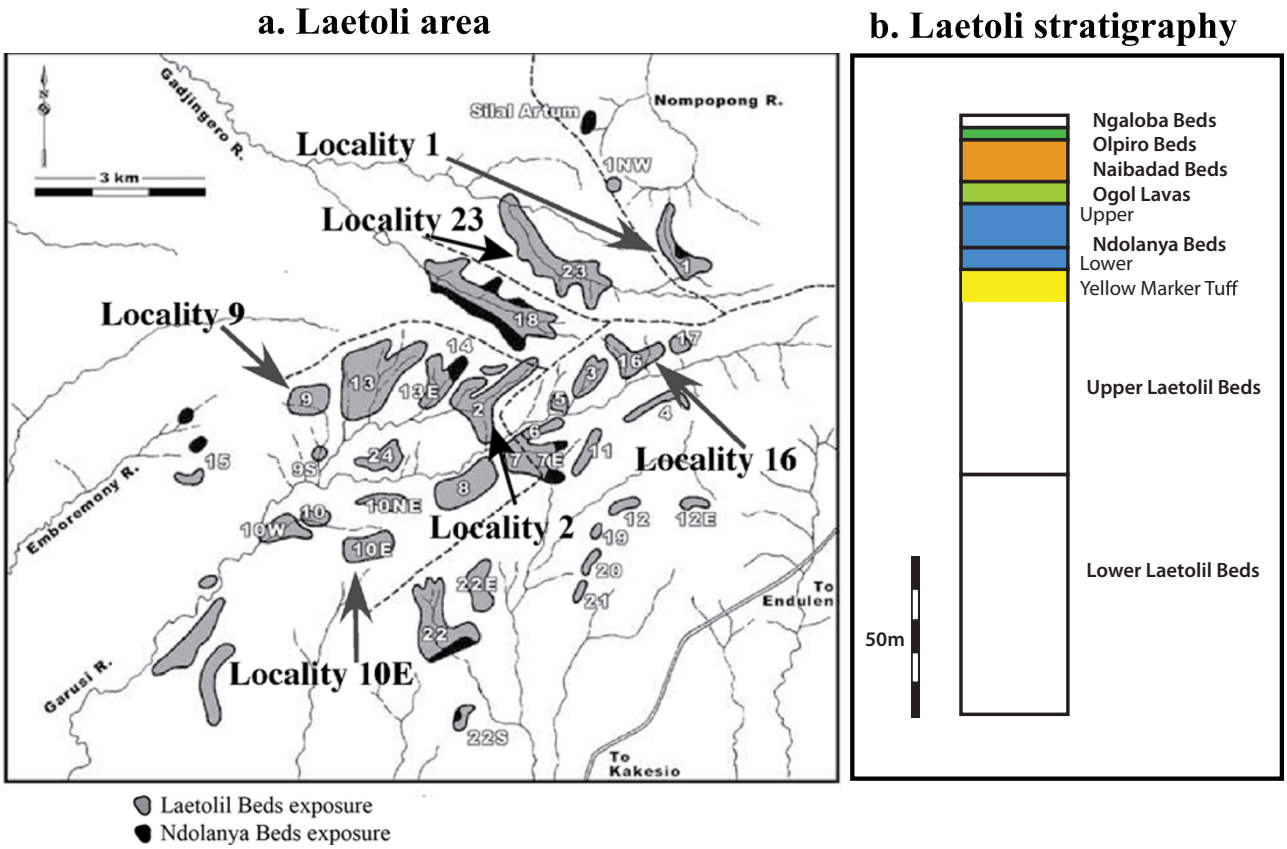

Figure 2. Map of Laetoli localities (a) and overview of Laetoli area stratigraphy (b), indicating extent of Laetolil and Ndolanya beds exposures and the positions of sites sampled in the current study (after McHenry, 2011).

artefacts (Day et al., 1980; Leakey, 1987c; Masao and Kimambo, 2021). The current work improves and expands upon the prior dating and tuff compositional analyses for the deposits in the Laetoli region that are younger than the Ndolanya Beds, with a focus on the Naibadad Beds, which overlap in age and in general composition (rhyolitic) with Ngorongoro volcano and the newly described Ngorongoro Formation recovered from OGCP cores at Olduvai (Njau et al., 2021).

https://doi.org/10.1017/qua.2025.17 Published online by Cambridge University Press

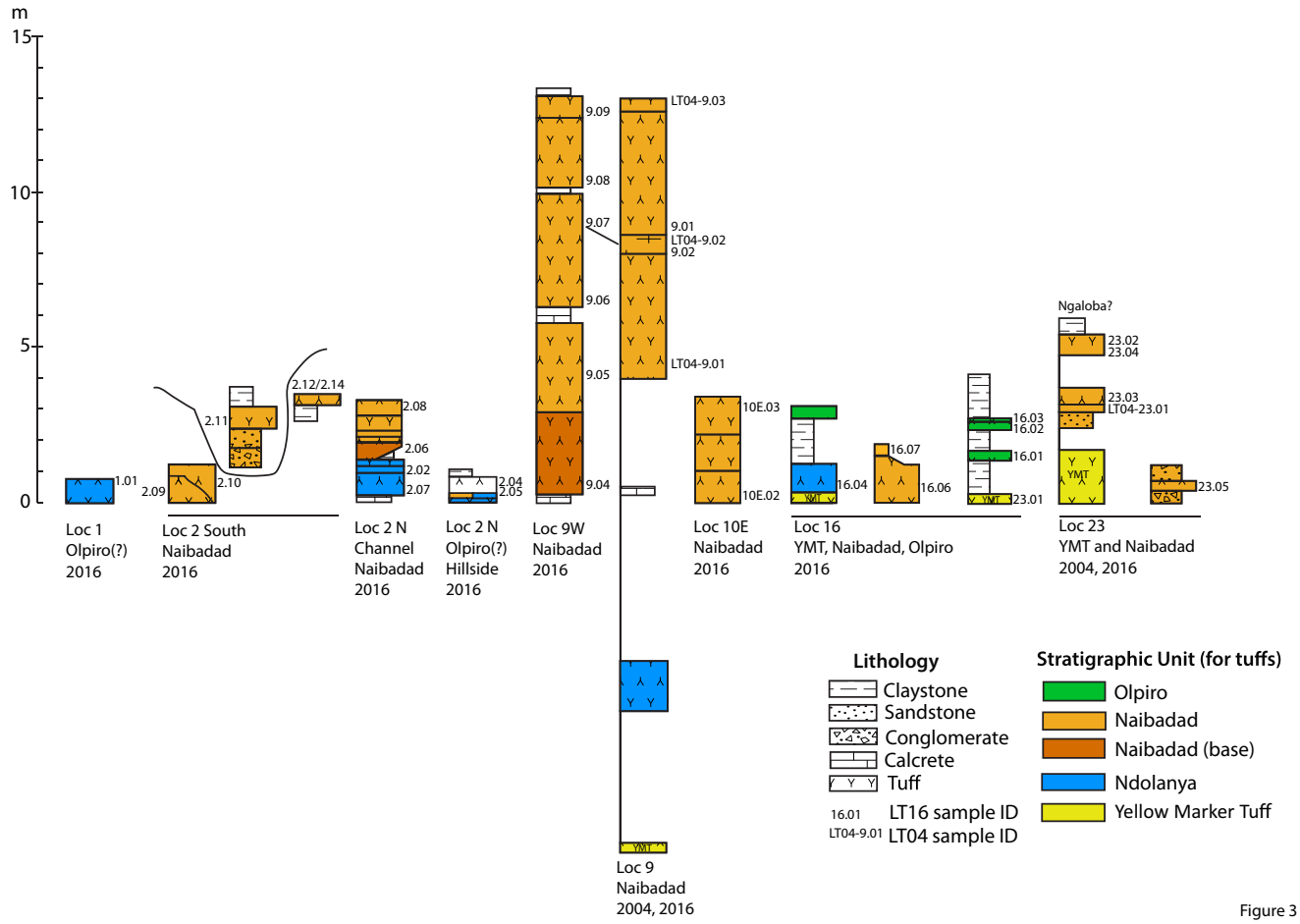

Figure 3. Measured stratigraphic sections, showing positions of samples collected. Color coded by bed (based on tephra composition). Sections are organized by locality number. Clusters of nearby stratigraphic sections are grouped, with a solid horizontal line beneath. No datum is implied by the positions of the bases of the stratigraphic sections. Section descriptions focused on relative positions of tephra layers, thus not all intervening lithologies were noted for all sites.

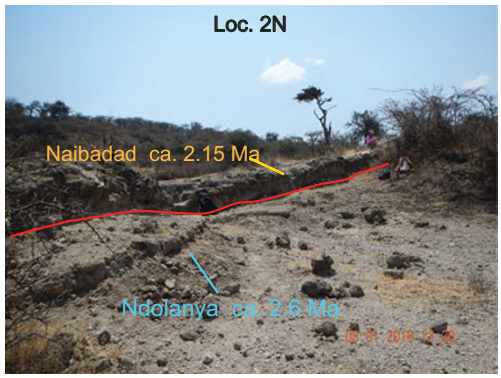

Figure 4. Locality 2N field photo showing the contact between the Ndolanya Beds and Naibadad Beds and positions of sampled tephra units.

Background

Geologically noteworthy localities within the Laetoli area were first enumerated in Hay (1987); those sites most relevant to the current study are highlighted in Figure 2. The Ndolanya Beds (Hay, 1987) unconformably overlie the Yellow Marker Tuff (YMT), which marks thept top of the Upper Laetolil Beds. The Lower Ndolanya Beds consist largely of pedogenically altered tuffaceous claystone with some tephra, while the Upper Ndolanya Beds are typified by clay-rich aeolian tuffs with some calcrete (Ditchfield and Harrison, 2011).

The Ogol lavas locally overlie the Upper Ndolanya Beds and consist of phaneritic to porphyritic vogesite or alkaline basalt, with olivine and augite phenocrysts in a feldspar and augite matrix (Hay, 1987; Mollel et al., 2011; Zaitsev et al., 2021). They have been variously interpreted as locally sourced lavas (Hay, 1987; Zaitsev et al., 2021) or as the erosional remnants of lava flows originating from Lemagurut volcano (Mollel et al., 2011).

The Naibadad Beds are younger than the Ogol lavas, although they are not found in direct superposition, except possibly at Locality 10E where their relative stratigraphic position remains ambiguous. The Naibadad Beds are principally tuff (> 95%), with minor claystone and conglomerate. The Naibadad Beds tuffs are trachytic to rhyolitic, with a likely Ngorongoro volcanic source (Hay, 1987; McHenry, 2011).

The Olpiro Beds are represented by relatively small, local exposures, identified by Hay (1987) at Localities 1, 16, and 23 and in unpublished theses by Ndessokia (1990) and Manega (1993) at a few additional sites (e.g., Locality 2S). The Olpiro Beds are dominated by brown claystone with minor conglomerate and sandstone,

https://doi.org/10.1017/qua.2025.17 Published online by Cambridge University Press

along with a tuff (the Olpiro Tuff). While Hay (1987) proposed a correlation between the Olpiro Tuff and Olduvai Bed II based on composition, more recent dating attempts have placed its age at > 2.0 Ma (Deino, 2011), which is much too old to support such a correlation since the base of Bed II is ca. 1.8 Ma (Deino, 2012). Mollel et al. (2011) proposed a correlation between the Olpiro Tuff and the Coarse Feldspar Crystal Tuff (CFCT) in Olduvai Bed I, but while the two are likely similar in age, a more detailed analysis of the CFCT (McHenry et al., 2020) revealed a dominantly rhyolitic composition unlike the trachytic composition of the Olpiro Tuff.

Recently published ages and tephra compositions for the OGCP cores collected from the nearby Olduvai basin in 2014 (McHenry et al., 2020; Deino et al., 2021), which include new stratigraphy below the level exposed in outcrop now referred to as the Ngorongoro Volcanic Formation (Stanistreet et al., 2020), provide an opportunity to correlate between Laetoli and the Olduvai basin. Tuffs and ignimbrites sampled in the lower part of Core 2A (below the Olduvai Bed I basalt) have trachytic to rhyolitic compositions and ages between 2.167 Ma and 2.003 Ma (Deino et al., 2021), comparable to previous results for the Naibadad Beds tuffs (e.g., Deino, 2011). Core 3A provides a similar record of Ngorongoro volcanism, with tuffs below the level of the Olduvai Bed I basalt dating from 2.112 to 2.030 Ma (Deino et al., 2021). The 2014 OGCP cores did not reach bedrock, and a seismic survey of the Olduvai basin (Lu et al., 2019) reveals that there is likely an additional 200+ meters of basin fill below the level cored, suggesting that older beds of Laetoli could have stratigraphic equivalents still buried deep within the Olduvai basin.

Field methods

Key Naibadad and Olpiro beds localities named and described by Hay (1987), Manega (1993), Ndessokia (1990), and McHenry (2011) were re-visited in 2016 for detailed stratigraphic measurement and tuff sampling (Figure 3). Tephra samples (LT16 prefixes, 35 samples total) and $^{40}Ar/^{39}Ar$ samples (L16 prefixes, 21 samples total) were collected in parallel by two of us (LM and AD, respectively).

Samples dated here are tuffs and lavas from Laetoli and nearby potential proximal tephra and source areas to the northeast (Naisuri Gorge and Lemagurut Volcano). All $^{40}Ar/^{39}Ar$ dating samples were collected by one of us (AD) during the 2016 field season. The dated sample set consists of 21 tuffs derived from the upper Ndolanya Beds, a tuff apparently related to the Ogol Lava in Naisuri Gorge, and the Naibadad Beds. In addition, we dated a sample of the Ogol Lava, and a lava exposed on the flanks of Lemagurut Volcano.

At Locality 2N (the northern end of Locality 2; see Figure 2A), exposures along the slope of the ridge to the north were scouted for claystone and darker-colored tephra potentially corresponding to the Olpiro Beds (from which two samples were collected), and lower-lying tuffaceous outcrops to the south of this ridge were measured and sampled for the Naibadad Beds (Figure 4, four samples collected). At Locality 2S (the southern end of Locality 2), we searched for Manega's (1993) purported Olpiro Beds exposure and measured a series of detailed sections of Naibadad Beds tuffs (five samples collected), some of which preserve volcanic glass. Figure 3 shows the erosional relationships among the three measured sections from this site.

At Locality 9 (Figure 2A) we collected tephra samples at sites 9W (six samples) and 9 (two new samples), the latter of which overlaps with the section previously analyzed in McHenry (2011). Tuff positions and thicknesses were measured from the top of the Yellow Marker Tuff (top of the Laetolil Beds) up through the Naibadad Beds (Figure 3). Section 9W, 700 meters to the west of Locality 9 along the same hillside, was measured and sampled from the base to the top of the exposure (~13 meters, all within the Naibadad Beds). The units identified in this section are almost entirely tuff, with calcretes separating most units.

Two Naibadad Beds tuffs were sampled from within a continuous stratigraphic section at Locality 10E (Figure 2A). The Ogol lava was sampled from the top of nearby Norsigidok Hill.

Locality 16 serves as the type locality for the Olpiro Beds because the Olpiro Tuff is best preserved and most easily identified here near its base (Hay, 1987). We collected three samples of the Olpiro Tuff, one sample of Ndolanya tuff, and two samples of Naibadad Beds tuffs at this locality, although complex unconformable stratigraphy made it impossible to collect from a single continuous section.

Hay (1987) also identified the Olpiro Beds at Localities 1 and 23, while Manega (1993) provisionally identified an exposure at Locality 2S. We visited these locations and collected samples from units matching the stratigraphic descriptions of the Olpiro Beds, when they could be located. Four samples from three distinct Naibadad tuffs and one sample of the Yellow Marker Tuff (topmost unit of the Laetolil Beds) were collected from Locality 23. One candidate Olpiro tuff was sampled from Locality 1.

We also visited and collected two samples at Naisuri Gorge, a steep valley incised through volcanic stratigraphy located to the east between Laetoli and Lemagurut, and from the summit of Lemagurut itself (Figure 1). These samples contribute to our understanding of the regional chronostratigraphy and potential source areas.

Laboratory methods

$^{40}Ar/^{39}Ar$ dating methods

The $^{40}Ar/^{39}Ar$ sampling and dating methods used here are similar to those used previously to date Laetoli tuffs (Deino, 2011), with modifications primarily related to the availability and use of a newer generation of Noble gas mass spectrometers with improved resolution, sensitivity, and multi-collection capability, as described below. Additional details as to the use of this equipment are provided in Deino et al. (2019a, 2019b). We also described a new approach to age estimation of central tendencies of replicate analyses of individual phenocrysts from a tuff, based on Bayesian inference (Deino et al., 2019b).

Samples were processed at the Berkeley Geochronology Center (BGC) in preparation for $^{40}Ar/^{39}Ar$ dating. The tuff processing methodology is similar to that described in Deino (2011), using conventional separation techniques consisting of disaggregation using a ceramic mortar and pestle, sieving, dilute HF and distilled water rinses, and hand-picking under a binocular microscope to obtain a finished product of clean feldspar grains as free of inclusions as possible.

The two lava samples were processed to obtain purified groundmass separates by hand crushing in a metal mortar and

https://doi.org/10.1017/qua.2025.17 Published online by Cambridge University Press

https://doi.org/10.1017/qua.2025.17 Published online by Cambridge University Press

Table 1. Summary of dating results

		Latitude	Longitude	Analytical				Weighted-Mean				Bayesian Model	
Sample	Lab ID	N°	W°	Method†	*n*	Ca/K§		Age (Ma ± 1 SD)‖		MSWD‡	Prob.	Age (Ma ± 1 SD)¶	
Naibadad Beds (upper)													
L16/23−2	79050	−3.190494	35.210260	SGIH	5/11	0.018	± 0.006	2.011	± 0.003	6.4	0.00	**2.004**	**0.003**
L16/2−1w	79057	−3.202791	35.192617	SGIH	5/8	0.029	± 0.031	2.115	± 0.032	1.2	0.00	**2.016**	**0.047**
9-NB3*	25168	−3.203221	35.167917	SCTF	12/21	0.015	± 0.005	2.057	± 0.017	6.6	0.00	**2.020**	**0.010**
L16/9w−5	79088	−3.208187	35.163134	SGIH	14/35	0.018	± 0.007	2.043	± 0.003	4.9	0.00	**2.036**	**0.003**
Naibadad Beds (middle)													
L16/9−1p	79054	−3.205340	35.168989	SGIH	7/10	0.041	± 0.004	2.112	± 0.002	2.8	0.00	**2.104**	**0.003**
L16/16−2	79058	−3.200730	35.213179	SGIH	13/19	0.031	± 0.015	2.150	± 0.008	6.0	0.00	**2.115**	**0.009**
L16/10−3	79045	−3.236663	35.169117	SGIH	6/8	0.021	± 0.012	2.124	± 0.002	10.0	0.00	**2.1175**	**0.0018**
9-NB2*	25169, 25170	−3.205506	35.169217	SCTF	15/21	0.047	± 0.027	2.155	± 0.012	3.6	0.00	**2.132**	**0.008**
Naibadad Beds (lower)													
L16/2s−1	79053	−3.218709	35.193822	SGIH	7/8	0.070	± 0.040	2.159	± 0.003	2.1	0.05	**2.154**	**0.003**
L16/10−2	79044	−3.236479	35.169112	SGIH	23/25	0.033	± 0.024	2.180	± 0.005	2.1	0.00	**2.163**	**0.007**
L16/16−1	79047	−3.200138	35.212843	SGIH	8/8	0.038	± 0.006	2.172	± 0.002	8.5	0.00	**2.1636**	**0.0020**
L16/2−2c	79062	−3.203999	35.191358	SGIH	16/17	0.030	± 0.006	2.188	± 0.005	3.9	0.00	**2.164**	**0.006**
L16/2−2d	79064	−3.203999	35.191358	SGIH	16/17	0.033	± 0.011	2.193	± 0.007	2.3	0.00	**2.172**	**0.009**
L16/2s−3	79068	−3.218855	35.193576	SGIH	15/17	0.045	± 0.016	2.191	± 0.008	1.1	0.06	**2.172**	**0.012**
L16/9w−1	79070	−3.208274	35.163162	SGIH	6/8	0.035	± 0.011	2.177	± 0.004	0.3	0.72	**2.175**	**0.005**
L16/23−3	79051	−3.190363	35.210134	SGIH	11/13	0.018	± 0.005	2.182	± 0.001	1.4	0.03	**2.178**	**0.003**
L16/2s−2	79066	−3.218942	35.193857	SGIH	15/19	0.026	± 0.005	2.189	± 0.003	0.7	0.17	**2.185**	**0.004**
L16/2s−4	79069	−3.218753	35.193402	SGIH	15/18	0.035	± 0.017	2.195	± 0.006	0.9	0.31	**2.189**	**0.008**

https://doi.org/10.1017/qua.2025.17 Published online by Cambridge University Press

Table 1. (*Continued.*)

		Latitude	Longitude	Analytical				Weighted-Mean				Bayesian Model	
Naisuri Gorge tuff													
L16/NSG−1	27580	−3.154204	35.238816	SGIH	2/24	0.219	± 0.147	2.334	± 0.017	0.2	0.65	**2.327**	**0.014**
Lemagrut (summit lava)													
L16/LEM−1	27690	−3.165616	35.360009	MGIH	1/1	0.507	± 0.000	**2.341**	**± 0.007**	1.0	1.00	—	—
Olgol Lava													
L16/10−1	27642	−3.235856	35.170593	MGIH	2/2	1.716	± 0.002	**2.308**	**± 0.013**	0.0	0.84	—	—
L16/10−1 HCl/HNO3	27684	−3.235856	35.170593	MGIH	2/2	1.249	± 0.146	**2.346**	**± 0.008**	0.3	0.61	—	—
								2.336	***0.017***				
Ndolanya Beds (upper)													
L16/2−1sw	79060	−3.202791	35.192617	SGIH	7/7	0.000	± 0.010	2.593	± 0.003	1.1	0.35	**2.590**	**0.004**
L16/1−1	79056	−3.191245	35.228524	SGIH	6/6	0.003	± 0.069	2.607	± 0.006	0.8	0.58	**2.604**	**0.006**
L16/2−2b	79061	−3.203999	35.191358	SGIH	14/16	0.010	± 0.009	2.648	± 0.004	2.3	0.00	**2.620**	**0.007**
L16/2−2a	79048	−3.203999	35.191358	SGIH	6/10	0.005	± 0.002	2.639	± 0.001	0.3	0.86	**2.6387**	**0.0014**
18-Nd2*	25187	−3.198087	35.197218	SCTF	12/12	0.009	± 0.010	2.660	± 0.016	0.9	0.52	**2.650**	**0.009**
												2.633	***0.008***

*Previously published in Deino, 2011.
†SCIH = single-crystal incremental heating; MGIH = multi-grain incremental heating; SCTF = single-crystal total fusion (Deino, 2011).
‡Mean square weighted deviation.
§Median Ca/K value.
‖Weighted-mean age ± 1 SD modified standard error (standard error multiplied by root MSWD when MSWD > 1).
¶Bayesian model age using exponential prior distribution ± 1 SD standard error.
Preferred ages shown in **bold** font.
Weighted-mean ages are shown in ***bold-italic*** font.

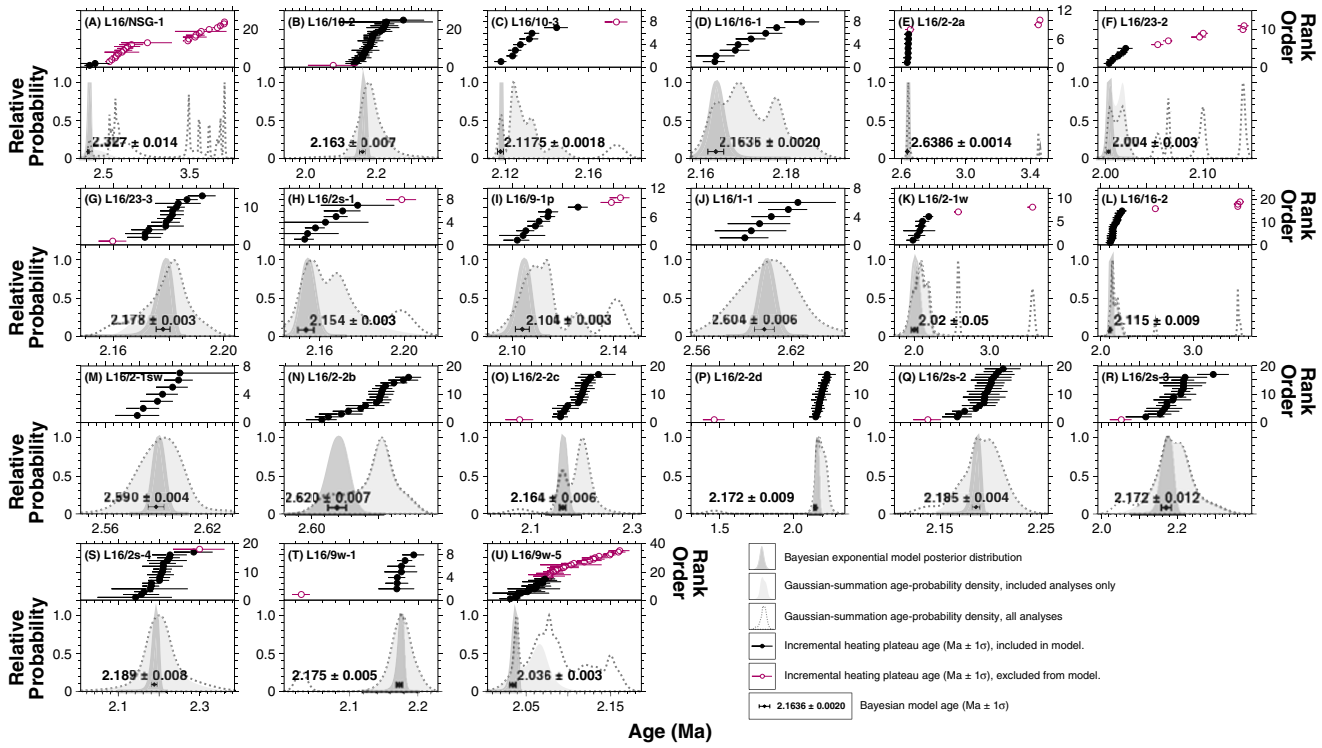

Figure 5. (A–U) Feldspar phenocryst SCIH age-probability distributions showing the age-probability density spectra of each dated tuff sample. Each plot shows the age distribution before outlier deletion, after outlier deletion, and the estimated Bayesian exponential model posterior distribution (see legend). A rank-order plot of each analysis is shown in the upper part of each graph.

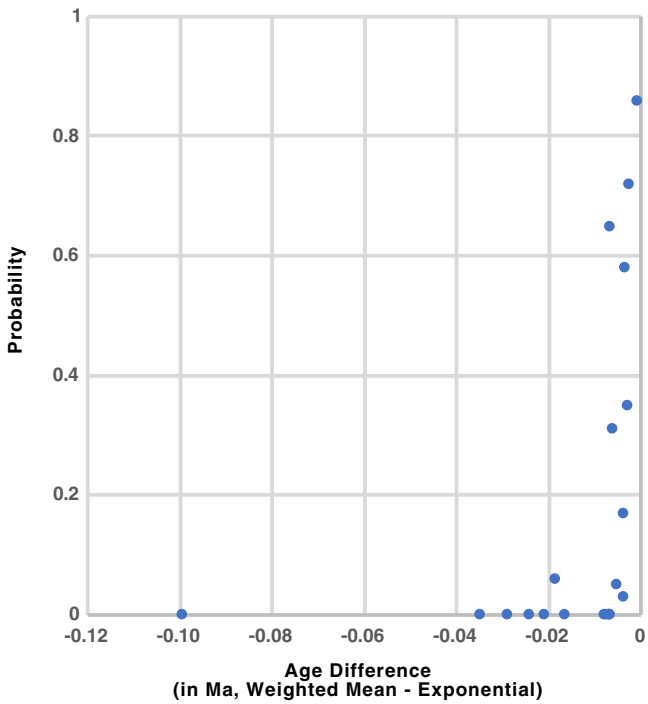

Figure 6. Mean square of weighted deviates (MSWD) probability versus age difference. Variation of the MSWD probability with the difference in age of a weighted-mean versus Bayesian exponential age estimation for individual sample age populations.

pestle, sieving (250–350 microns for Ogol Lava sample L16/10, and 150–250 microns for Lemagurut sample L16/LEM-1), removal of phenocrysts with a hand magnet, a magnetic Frantz Isodynamic Separator, separation with heavy liquids, and hand-picking. This was followed by several rinses in distilled water in an ultrasonic bath. As an experiment to see if the radiogenic content and argon systematics could be improved by acid treatment, a split of the Ogol Lava sample ('L16/10 HCl/HNO3') was treated with a sequence of mild acid washes (HCl 1N, HCl 6N, HNO_3 1N, HNO_3 6N) at 60°C in an ultrasonic bath prior to the final distilled water rinse to potentially remove alteration products.

The final mineral separates were irradiated in the cadmium-lined in-core irradiation tube (CLICIT) position of the Oregon State University TRIGA reactor in three batches (BGC irradiation 471 for 0.83 hour, and 474 and 478 for three hours each). All irradiations employed sanidine phenocrysts from the Alder Creek Rhyolite of California (orbitally referenced age = 1.1848 ± 0.0006 Ma; Niespolo et al., 2017) as the neutron fluence monitor mineral. Standards and unknowns were co-irradiated in a circular configuration in wells in an aluminum disk, with standards at the cardinal positions, and either two or three unknowns situated between standards. The appropriate neutron fluence factor (the '*J*' parameter of $^{40}Ar/^{39}Ar$ dating calculations; McDougall and Harrison, 1999) for the unknown positions was calculated from a planar fit of the standard calibrations, with 1σ errors derived by Monte Carlo simulation in the predicted *J* value ranging from 0.1–0.3%. Reactor-induced isotopic production ratios for these irradiations were: $(^{36}Ar/^{37}Ar)_{Ca} = 3.65 \pm 0.02 \times 10^{-4}$, $(^{38}Ar/^{37}Ar)_{Ca} = 1.96 \pm 0.08 \times 10^{-5}$, $(^{39}Ar/^{37}Ar)_{Ca} = 6.95 \pm 0.09 \times 10^{-4}$, $(^{37}Ar/^{39}Ar)_{K} = 3.24 \pm 0.16 \times 10^{-4}$, $(^{38}Ar/^{39}Ar)_{K} = 1.220 \pm 0.003 \times 10^{-2}$, $(^{40}Ar/^{39}Ar)_{K} = 3.5 \pm 0.9 \times 10^{-4}$. Atmospheric $^{40}Ar/^{36}Ar = 298.56 \pm 0.31$ (Lee et al., 2006) and decay constants follow (Min et al., 2000).

https://doi.org/10.1017/qua.2025.17 Published online by Cambridge University Press

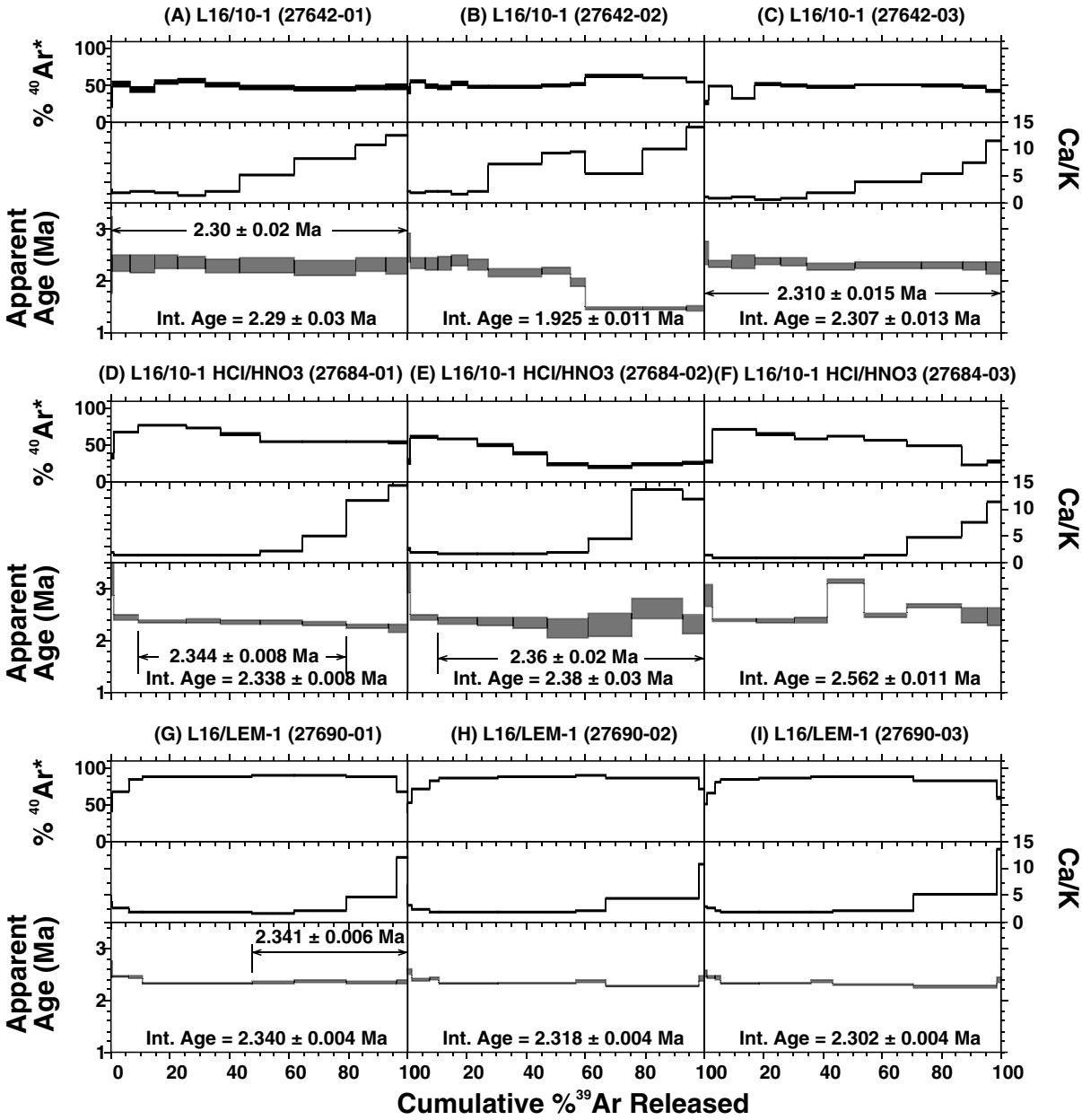

Figure 7. (A–I) Lava flow matrix groundmass using incremental heating (MGIH) incremental ^{39}Ar release spectra showing ^{39}Ar incremental release spectra for three aliquots each from three lava samples. 'Int. Age' at the bottom of each panel provides the integrated age from computational re-combination of all gas steps. Apparent-age plateaus are shown by the double-barbed arrows. All uncertainties are 1σ analytical error.

After a period of several months to permit radiological 'cooling' after irradiation, the materials were analyzed at the BGC using two techniques. K-feldspar phenocryst separates were analyzed grain-by-grain, and each grain was tested using incremental heating. Here, heating levels (laser output levels) were raised progressively from low temperature to fusion in a series of sequential independently measured steps (4–10 steps), termed the single-crystal incremental heating (SCIH) approach. To conserve analytical resources, grains yielding ages much older than expected in the first two steps were not analyzed further. The two lava samples (three separates) were analyzed in three small (10–20 mg) multi-grain aliquots per sample of groundmass using incremental heating ('MGIH'). All argon measurements were carried out using an automated extraction line leading to a Nu Instruments 5-collector Noblesse mass spectrometer, using ion-counting electronics.

Completed incremental heating analyses were checked for apparent age plateaus, using a modified approach to that of Fleck et al. (1977). Here, we searched for a set of contiguous steps encompassing the greatest percent of ^{39}Ar release that exhibited an acceptable MSWD ('mean square of weighted deviates,' with a threshold probability $> 95\%$ that the observed scatter is caused by analytical error alone and that geological scatter is not demonstrated). A plateau must comprise at least 50% of the total ^{39}Ar release and consist of at least three consecutive steps. We added

https://doi.org/10.1017/qua.2025.17 Published online by Cambridge University Press

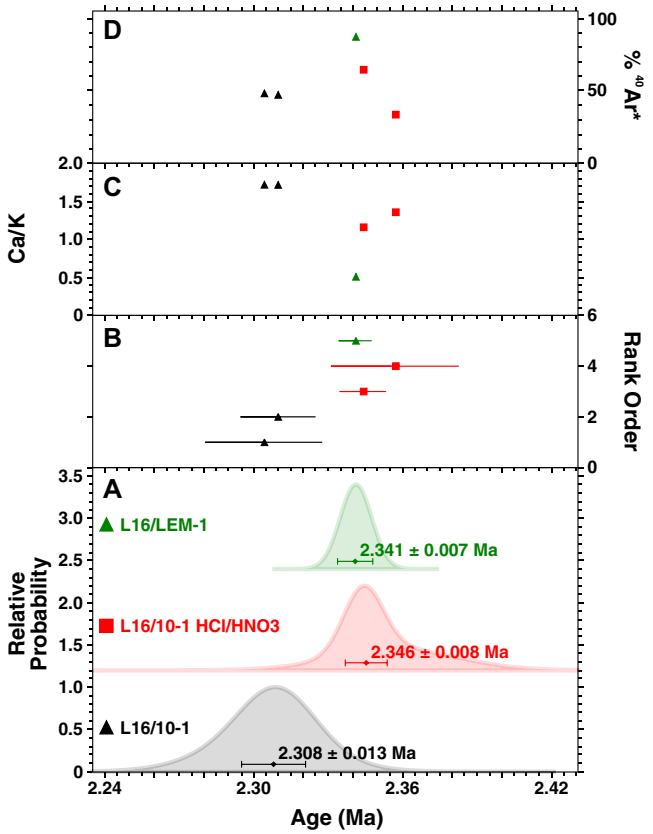

Figure 8. Groundmass using incremental heating (MGIH) age-probability spectra and related parameters. (A) Age-probability density spectra of each sample, with weighted-mean age and 1σ error (including error in *J*, the neutron fluence parameter in $^{40}Ar/^{39}Ar$ dating). (B) Rank order plot of the individual aliquots grouped by sample. Uncertainties in age are given at 1σ standard error. (C) Ca/K atomic ratio derived as a by-product of the $^{40}Ar/^{39}Ar$ analysis. (D) Percentage of radiogenic ^{40}Ar released.

here an additional threshold for inclusion of a plateau in further data analysis, in that the overall experiment must have consisted of more than three steps.

We further analyzed the argon systematics using 'inverse isochron' regressions ($^{36}Ar/^{40}Ar$ vs. $^{39}Ar/^{40}Ar$) calculated from the plateau steps (Tables S1 and S2). However, we present these results, in the form of $^{40}Ar/^{36}Ar$ 'trapped' composition and isochron age, for comparison only. In the more highly radiogenic data suites from older, relatively highly potassic samples such as these, we find that isochrons either reproduce the plateau ages within error, or introduce anomalous scatter to age populations; thus, the plateau age is taken as the reference age of all incremental heating analyses.

The age populations for a given sample were examined for outliers using a two-step approach. Age outliers may have either a geological origin (e.g., detrital contamination, alteration, or trapped excess ^{40}Ar), or be due to random analytical occurrence. Typically, a geological outlier is older than the primary eruption age of a tephra. We identified distinctly older grains using a gap-finding technique (Deino et al., 2019a, b), with the sensitivity set to a gap score of seven. This procedure is sufficient to flag most old outliers easily identified by a human observer yet have little effect on the primary age distribution. Secondly, we identified outliers by examining the deviation of results from the median age and omitted those with a normalized median absolute deviation ('nMAD') from the median > 3.

Finally, we present two approaches to calculating the central tendency and error of the filtered sample age populations. The first calculates a conventional weighted mean, with the error as a modified standard error (multiplied by root MSWD where the MSWD > 1). The second uses a Bayesian parameter estimation approach (Keller, 2018; Deino et al., 2019b) that accommodates a tailing toward older ages commonly observed in East African phenocrystic feldspar phenocryst $^{40}Ar/^{39}Ar$ single-crystal data sets from tuffs (e.g., Deino et al., 2019b). Such tailing is evident here in several samples (e.g., L16/2s-1 and L16/16-1). Our Bayesian prior constraint centers on the assertion that, although inherited, xenocrystic, or detrital grains may predate deposition, no $^{40}Ar/^{39}Ar$ ages may postdate deposition, except due to analytical uncertainty. Consequently, we expect a relative distribution of true single-crystal closure ages that is truncated at the time of deposition. The majority of ages should cluster at this limit within analytical uncertainty; however, the proposed distribution should permit a tail of older ages from, for example, incompletely degassed xenocrysts. We found that an exponential decay model meets this requirement, and closely approximates the conventional weighted mean when excess analytical scatter is absent.

Electron probe microanalysis methods

For electron probe microanalysis (EPMA), samples were gently crushed in a ceramic mortar and pestle, sieved to obtain the 60–100 mesh size fraction, sonicated in a 4% HF solution for one minute, and rinsed a minimum of three times in DI water (until the decanted solution was clear). Where identified, individual grains of feldspar, augite, hornblende, glass, oxide minerals (ilmenite and titanomagnetite), olivine, aenigmatite, and andradite (melanite) garnets were then hand-picked under a microscope and mounted in epoxy, polished, carbon coated, and analyzed by electron microprobe (Cameca SX-Five at University of Wisconsin-Madison). Phase identifications were confirmed using energy dispersive spectroscopy (EDS), and then quantitatively analyzed using phase-specific routines by wavelength dispersive spectroscopy (WDS) following the methods described in McHenry et al. (2016). Check samples (including glass, feldspar, augite, hornblende, and titanomagnetite) were analyzed at the start of every run, with calibrations adjusted to ensure consistency between runs. Specific analytical details, including beam parameters, standards, and check sample compositions, are reported in McHenry et al. (2020).

Correlation methods

Tuffs were characterized compositionally using two main approaches: (1) presence/absence of specific minerals and (2) EPMA elemental data of selected phases. The presence/absence and qualitative relative abundance of minerals were determined using optical microscopy during hand picking for EPMA analysis and confirmed by EPMA. The elemental compositions of the analyzed augite, titanomagnetite, feldspar, and (where available) glass and hornblende of various samples were compared visually using a series of bivariate and ternary plots, looking for compositional clusters. A correlation is possible where mineral assemblage (presence/absence of phases) and compositional clustering across multiple phases agree, although with closely spaced, compositionally similar tuffs, this does not always produce a unique "fingerprint" for an individual eruption.

https://doi.org/10.1017/qua.2025.17 Published online by Cambridge University Press

Table 2. Sample IDs, bed designations, and mineral assemblages

Ar sample	Tuff sample	Site	Expected	Age	Composition	Augite			Feldspar			Oxides				Glass				Other							
						Na, Fe rich	Na, Fe-poor	Fe-rich, Na-poor	High-K	Anorthoclase	Plagioclase	High-Ti Ti-mag	Low-Ti Ti-mag	Ilmenite	Rhyolite	Rhyolite/ Trachyte	Trachyte	Basalt	Andradite	Hornblende	Olivine	Titanite	Perovskite	Biotite	Aenigmatite
Locality 1																											
L16/1−1	LT16−1.01	1	Olp	Ndo	Ndo	XX	XX		XX	+									X								
Locality 2																											
L16/2−2b	LT16−2.02	2N	Ndo	Ndo	Ndo	XX			XX	X			X									+					
L16/2−1w	LT16−2.04	2N	Olp	U Naib	Ndo	XX			XX	XX			XX						XX								
L16/2−1sw	LT16−2.05	2N	Olp	Ndo	Ndo	XX	X		XX		+		XX						XX								
L16/2−2c	LT16−2.06	2N	Naib	L Naib	Naib, Ndo	XX	X	+		XX	+	+					XX		XX								
L16/2−2a	LT16−2.07	2N	Ndo	Ndo	Ndo	XX	+		+	XX	+		XX				+										
L16/2−2d	LT16−2.08	2N	Naib	L Naib	Naib			XX		XX		XX					XX				XX						
L16/2s−2	LT16−2.09	2S	Naib	L Naib	Naib, Ndo	XX	XX			XX	X		XX						XX		+		+	+			
	LT16−2.10	2S	Naib		Naib, Ndo	XX		XX		XX		X	+	+				X	+		XX						
L16/2s−1	LT16−2.11	2S	Naib	L Naib	Naib, Ndo	XX	XX			XX	XX	+		+			+		XX								
L16/2s−3	LT16−2.12	2S	Naib	L Naib	No chem																						
L16/2s−4	LT16−2.14	2S	Naib	L Naib	Naib	+		XX		XX		XX				XX			X	+	XX		+				
Localities 9/9W																											
	LT16−9.01	9	Naib		Naib			XX		XX		+		XX	XX												
L16/9−1p	LT16−9.02	9	Naib	M Naib	few		+	+		XX				+		XX											
L16/9w−1	LT16−9.04	9W	Naib	L Naib	Naib, Ndo	XX	+			XX	X	XX	+			XX			XX		XX						
	LT16−9.05	9W	Naib		Naib	+	+	XX		XX		XX	+	X		XX			+								
	LT16−9.06	9W	Naib		Naib			XX		XX	+	XX				XX					X						
	LT16−9.07	9W	Naib		Naib			XX		XX		XX				XX				+							
	LT16−9.08	9W	Naib		Naib			XX		XX		XX		X		XX					X						
L16/9w−5	LT16−9.09	9W	Naib	U Naib	Naib	+	+	XX		XX		+		XX		XX					+						

(*Continued*)

https://doi.org/10.1017/qua.2025.17 Published online by Cambridge University Press

Ar sample	Tuff sample	Site	Expected	Age	Composition	Augite			Feldspar			Oxides			Glass				Other							
						Na, Fe rich	Na, Fe-poor	Fe-rich, Na-poor	High-K	Anorthoclase	Plagioclase	High-Ti Ti-mag	Low-Ti Ti-mag	Ilmenite	Rhyolite	Rhyolite/ Trachyte	Trachyte	Basalt	Andradite	Hornblende	Olivine	Titanite	Perovskite	Biotite	Aenigmatite
Locality 16																									
	LT16–16.01	16	Olp		Olp	+	XX			+	XX	XX					XX			XX					
	LT16–16.02	16	Olp		Olp		XX				XX	XX					XX			XX			+		
	LT16–16.03	16	Olp		Olp		XX			+	XX	XX					+			XX					
	LT16–16.04	16	Ndo		Ndo	XX	XX		XX		+		XX						X			X			
L16/16–1	LT16–16.06	16	Naib	L Naib	Naib	XX		XX		XX		XX			XX				X	+	XX				
L16/16–2	LT16–16.07	16	Olp	M Naib	few	X	+									XX									
Locality 10																									
L16/10–2	LT16–10E.02	10E	Naib	L Naib	Naib, Ndo	XX	XX			XX	+	XX	+	+		XX			X	+			+		
L16/10–3	LT16–10E.03	10E	Naib	M Naib	Naib			XX		XX	+	XX				XX				+	X				
Locality 23																									
	LT16–23.01	23	YMT		YMT	XX	XX			XX			XX						XX						
L16/23–2	LT16–23.02	23	Naib	U Naib	Naib			XX		XX	+	XX		+	XX				+		+				+
L16/23–3	LT16–23.03	23	Naib	L Naib	Naib, Ndo	XX	XX			XX						XX			+		+				
	LT16–23.04	23	Naib		Naib, Ndo	XX	+	XX		XX	X	XX	+	+	XX	+			XX		X		+		X
	LT16–23.05	23	Naib			XX	XX	XX		XX		XX	XX	+	XX				XX		XX				
Naisuri Gorge																									
L16/NSG–1	LT16-NS.01	Naisuri	Naisuri			X	XX		XX		+								XX				+		
	LT16-NS.03	Naisuri	Naisuri				XX				XX	XX		+						XX	X				

Mineral assemblages based on EPMA results on thin sections and grain mounts
XX = abundant; X = common; + = trace
Olp = Olpiro; Ndo = Ndolanya; Naib = Naibadad; L, M, U = Lower, Middle, Upper.

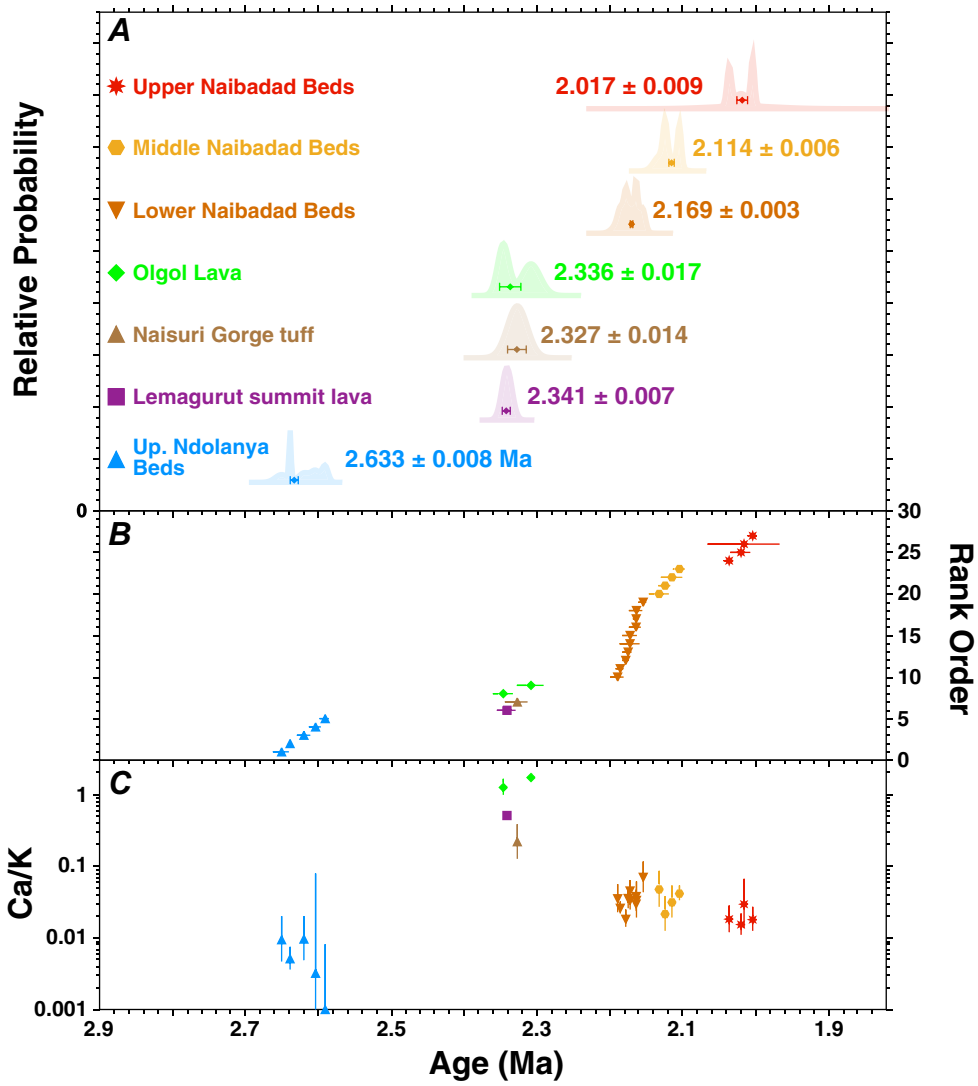

Figure 9. Summary age distribution of latest Pliocene–Pleistocene volcanism of the Laetoli area. These plots display all $^{40}Ar/^{39}Ar$ ages on upper Laetoli stratigraphic units, including three ages recalculated from Deino (2011). (A) Age-probability spectra combining samples for each stratigraphic unit, with weighted-mean unit age. Note that stratigraphic units may be composed of multiple eruptions separated in time, which have not been individually characterized. (B) Rank order of each sample grouped by stratigraphic unit. (C) Ca/K ratio of each sample. The volcanic source for tephra between ca. 2.2 and 2.0 Ma is identified as Ngorongoro volcano, while tephra and flows at ca. 2.3 Ma are from Lemagurut volcano. The volcanic source of the upper Ndolanya Beds remains enigmatic.

Results

$^{40}Ar/^{39}Ar$ dating results

The 1991 steps on 386 feldspar phenocrysts from 33 tuff samples were analyzed by the SCIH method (Table S1). Of these experiments, 40 were either truncated for the sake of efficiency after one or two initial low-power steps because they were much older than the expected eruption age or did not yield more than three steps prior to completion of the incremental heating release. The remaining experiments generally yielded plateaus (304 out of 346), 88% of these encompassing more than 90% of the total ^{39}Ar released (Table S2). After outlier detection and elimination from the plateau sample age populations as described in Methods, about half the samples are represented by simple, pseudo-normal distributions, while the others exhibit positive skewness (tail toward older ages) or pronounced multi-modality. Weighted-means of the plateau age populations are provided in Table 1.

More than half of the samples exhibit greater scatter than expected from analytical error alone (high MSWD with $>$ 95% probability that analytical error is insufficient to explain the observed dispersion). To provide a consistent approach to estimating a 'best' eruption age for these samples, we resorted to a Bayesian approximation technique utilizing an exponential prior distribution following Keller (2018) and Deino et al. (2019b). The estimated ages and probability distributions are shown in Figure 5 and listed in Table 1. The Bayesian parameter estimation approach yields ages that are in all cases younger than the weighted-mean ages, by a median of ca. 7 ka (minimum 0.8 ka, maximum 99 ka). Figure 6, illustrating the age difference as a function of the MSWD probability, shows that as the probability that analytical scatter alone is responsible for the observed distribution approaches zero, the age difference increases. This reflects the inappropriateness of the weighted-mean calculation, which assumes normality, while the Bayesian estimation approach emphasizes the younger end of the distribution as representing the true eruption age.

https://doi.org/10.1017/qua.2025.17 Published online by Cambridge University Press

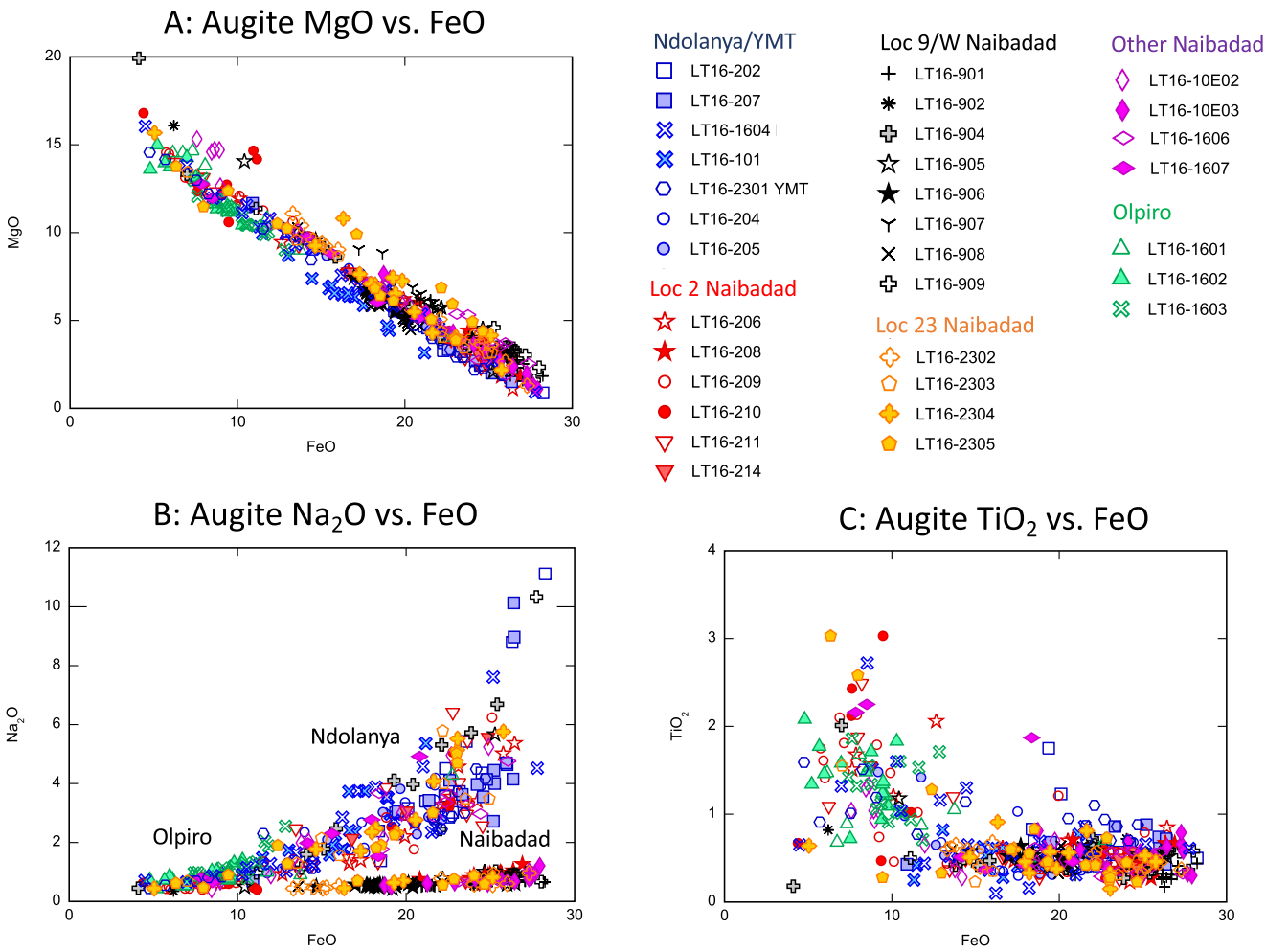

Figure 10. Electron probe microanalysis (EPMA) of augite compositions for samples collected in this study. (A) MgO versus FeO. This plot shows that Olpiro tuffs (green symbols) have higher Mg augite than most Ndolanya (blue symbols) or Naibabad tuffs (all other colors) and contain no high-FeO augite. (B) Na_2O versus FeO. This plot shows a distinctive low-Na augite population found within all Naibadad Beds tuffs (and absent in Ndolanya and Olpiro Beds tuffs), and that Olpiro Beds augite are low in FeO. (C) TiO_2 versus FeO, showing elevated Ti for the Olpiro Beds augite.

Eighty-nine steps on three aliquots each from three lava samples were analyzed by the MGIH method (Table S1). Incremental heating plateau and isochron data are provided in Table S2. Most MGIH aliquots yielded plateaus by the definition given above (5 of 9 experiments; Figure 7). The $^{40}Ar/^{36}Ar$ 'trapped' ratios derived from isochron analysis of the plateau steps are all within error of the anticipated atmospheric composition of 298.56 (Table S2; Lee et al., 2006), suggesting that inherited radiogenic ^{40}Ar is not a detectable problem with these samples. Age-probability spectra of the MGIH experiments are shown in Figure 8.

The two sample treatments on the Ogol Lava sample, one washed only in distilled water (L16/10-1) and the other treated with a series of warm HCl and HNO_3 washes (L16/10-1 HCl/HNO_3) as described in Methods, yielded distinctly different ages; acid washing increased the plateau ages slightly from a weighted mean of 2.308 ± 0.013 to 2.346 ± 0.008 Ma, a statistically significant difference at the 95% confidence interval. It is not readily apparent from the ^{39}Ar release spectra in Figure 8 which treatment yielded the most well-behaved argon systematics. The untreated material maintained greater consistency over the entirety of the release experiments, as reflected in the percentage of radiogenic ^{40}Ar, the Ca/K ratio, and the extent of the plateaus. However, the acid-treated material shows a sharper division in Ca/K behavior between what is likely matrix outgassing in the early phase of the experiment, and plagioclase/pyroxene outgassing in the latter third or so of the release. In the absence of a compelling reason to choose one sample treatment over another, we take the weighted-mean of the two treatments of 2.336 ± 0.007 Ma as the representative age of the Ogol Lava. The age of lava sample (L16/LEM-1) obtained from the summit of Lemagurut Volcano is 2.341 ± 0.007 Ma, on the basis of a single plateau result from the three MGIH experiments. The $^{40}Ar/^{36}Ar$ age results are summarized in Figure 9 and are described in detail in the discussion.

Electron probe microanalysis (EPMA) results

The mineral assemblages for the tuffs analyzed in this study are reported in Table 2. Phenocryst and glass compositions for the tuffs analyzed in this study are reported in S3–S10.

Examining the presence/absence data, together with the EPMA bivariate plots, several key clusters were observed that can be used to discriminate individual (or groups of similar) tuffs. While all samples contained some specific phases (e.g., feldspar of some kind, and augite), few samples contained abundant hornblende

https://doi.org/10.1017/qua.2025.17 Published online by Cambridge University Press

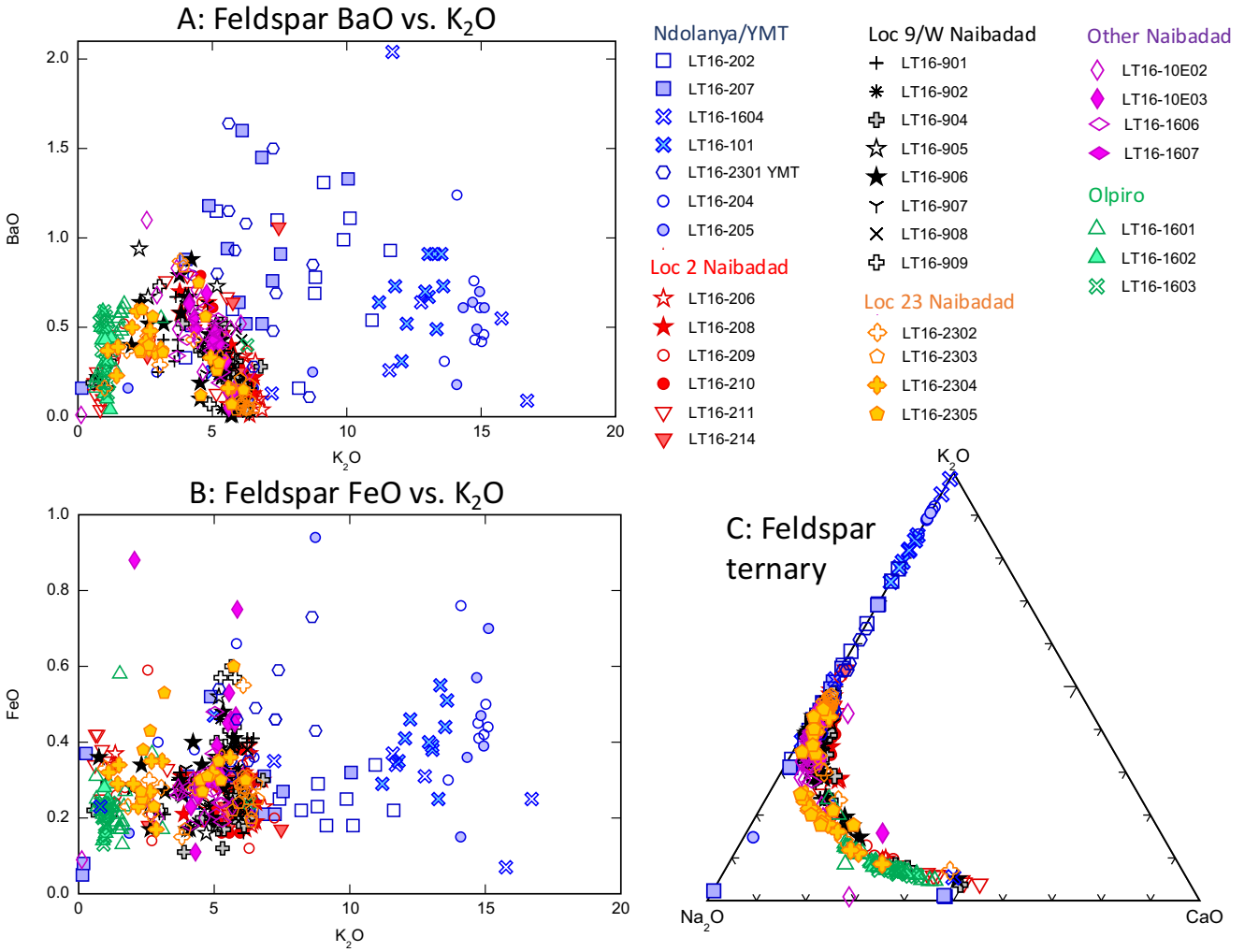

Figure 11. Electron probe microanalysis (EPMA) of feldspar compositions for samples collected in this study. (A) BaO versus K_2O. This plot shows compositional differences among the Olpiro (green symbols), Ndolanya (blue symbols), and Naibadad Beds feldspar, mostly in their K_2O content. (B) FeO versus K_2O, showing similar separations. (C) Feldspar ternary diagram, showing sanidine composition for Ndolanya Beds feldspar, anorthoclase for Naibadad Beds, and plagioclase for Olpiro Beds.

(only LT16-16.01, 02, and 03), and andradite garnet varied considerably in abundance between samples (e.g., not present in most Locality-9 samples, except for the basal Naibadad tuff). Augite was ubiquitous in the tuffs sampled but differed in composition (Figure 10), with distinct clusters characterized by low Na/high Fe, low Na/low Fe/high Ti/high Mg, and high Na/high Fe, although some samples contained more than one of these compositional groups. Feldspars also showed distinct compositional clusters (Figure 11), with some plotting as high-K sanidine (e.g. LT16-16.04, 1.01, 2.05, 2.04, 23.01), some intermediate plagioclase (e.g. LT16-16.01, 16.02, 16.03), and most in the anorthoclase compositional range. For samples that preserved glass, rhyolites LT16-23.02, 23.04, and 9.09 had the highest Si and lowest Al (Figure 12), while samples LT16-16.01 and 16.02 had the highest Al and plotted in the trachyte range. The glasses of samples LT16-9.04 and 2.08 overlap in composition (but not with other samples), suggesting a possible correlation.

For samples of uncertain stratigraphic origin (e.g., prospective "Olpiro Tuff" samples from sites other than Locality 16), the assemblage was compared against previously reported compositions for different beds within the Laetoli area (Hay, 1987; McHenry, 2011). While Naibadad Beds samples had mostly consistent mineral assemblages (rhyolitic or trachytic glass, anorthoclase feldspar, augite), most candidate "Olpiro Tuff" samples yielded compositions more similar to either Ndolanya or Naibadad beds tuffs, lacking the hornblende expected for the Olpiro Tuff.

Discussion

New chronostratigraphic groups for upper strata at Laetoli, based on $^{40}Ar/^{39}Ar$ dating results

Figure 9 and Table 1 summarize the overall age results for samples of the younger strata at Laetoli, from the Upper Ndolanya Beds through the Naibadad Beds, including three ages from Deino (2011) recalculated using the Bayesian approach described here for consistency. The ages determined for the tuffs of the Naibadad Beds can be grouped into three main intervals, with ten samples falling into the "Lower" (2.189–2.154 Ma), four in the "Middle" (2.115–2.104 Ma), and four in the "Upper" Naibadad Beds (2.036–2.004 Ma). Within these groups, ages mostly overlap

https://doi.org/10.1017/qua.2025.17 Published online by Cambridge University Press

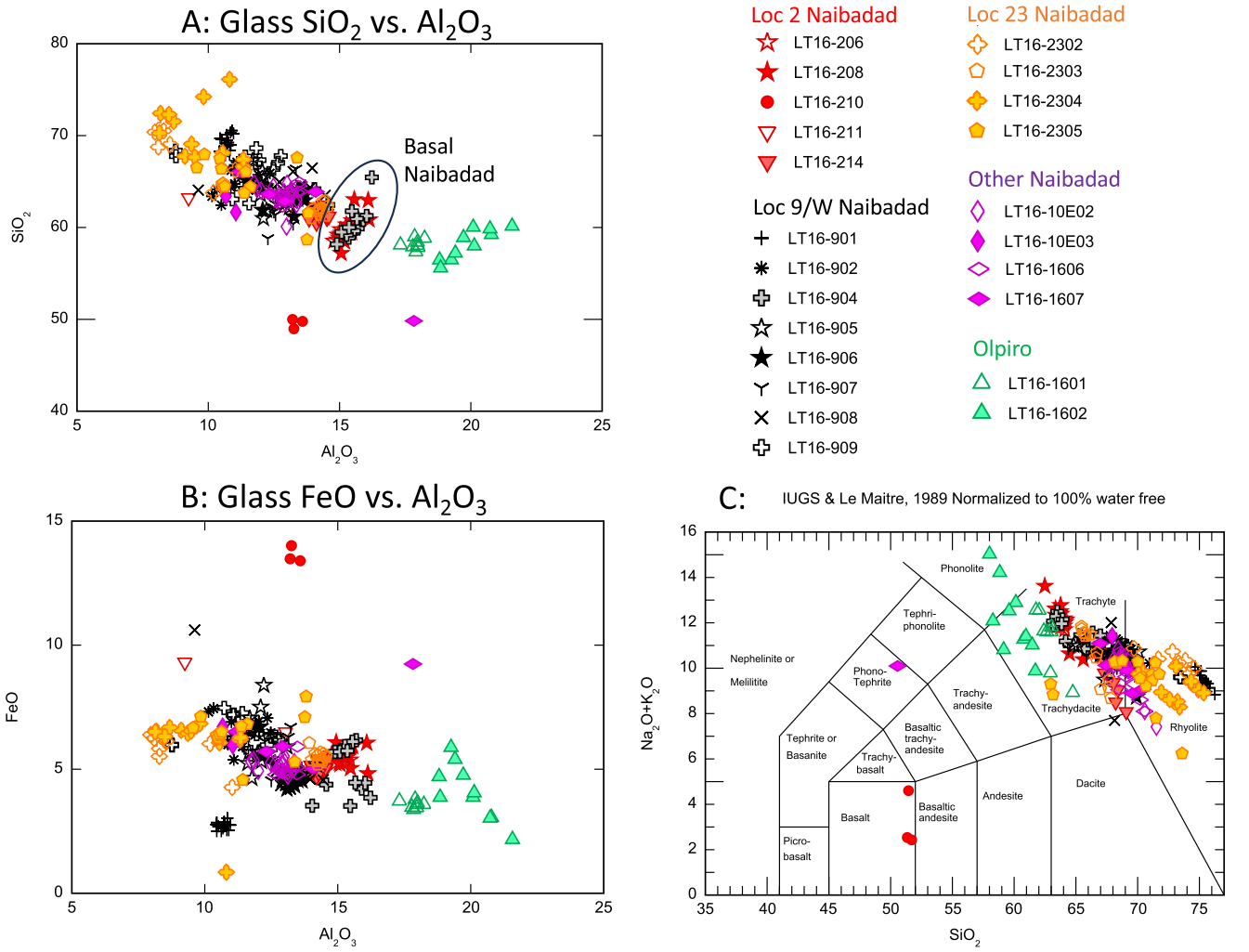

Figure 12. Electron probe microanalysis (EPMA) of glass compositions (EPMA) for samples collected in this study that preserve glass. (A) SiO_2 versus Al_2O_3. Olpiro glass (green symbols) has the highest Al, while Upper Naibadad samples LT16-23.02 and 23.04 have the highest SiO_2. (B) FeO versus Al_2O_3. (C) Alkali versus silica diagram, showing trachytic to phonolitic composition for Olpiro Beds and trachytic to rhyolitic composition for the Naibadad Beds glass. IUGS and Le Maitre, 1989. IUGS = International Union of Geological Sciences. No Ndolanya Beds samples collected for this study preserved volcanic glass.

within error; however, each group may be composed of several distinct eruptions separated by a short interval. While some sampled sites contain only Lower Naibadad Beds units (e.g., Localities 2, 2S), others contain units in more than one age group (e.g., Locality 16, Lower and Middle; Locality 10E, Lower and Middle; Locality 23, Lower and Upper; and Localities 9 and 9W, Lower, Middle, and Upper).

Compositionally, the Ca/K ratios are notably uniform within each age group but differ significantly between several of the groups. This observation suggests that each group has a unique volcanic source, but that sources shifted and evolved through time. For example, the oldest group, the Upper Ndolanya Beds, exhibits unusually low Ca/K ratios typical of high-K anorthoclase. Based on ages, and mineral compositional data described below, the tuffs of the Naibadad Beds are attributed to eruptions from the Ngorongoro Crater volcanic system, but the source of the ca. 300-kyr-older Upper Ndolanya Beds remains unknown. Finally, the anorthoclase composition trends toward decreasing Ca/K ratio from the Lower Naibadad Beds through the Upper Naibadad Beds and provides an intriguing hint of long-term evolution of the Ngorongoro Crater volcanic system (from ca. 2.2 to 2 Ma), the presumed source of these eruptions.

Relative timing of the Ogol Lavas and Lemagurut volcano

The age of the Lemagurut summit lava sample (L16/LEM-1) is 2.341 ± 0.007 Ma, which is statistically indistinguishable from that of the Ogol Lava age (2.336 ± 0.007 Ma) at the 95% confidence interval. These are not the same eruptions based on lithologic characteristics (e.g., L16/LEM-1 has large phenocrysts of plagioclase, which the Ogol Lava lacks, and the latter is characterized by abundant phenocrysts of pyroxene and olivine in LEM-1). Nevertheless, the age correspondence of late-erupted events from Lemagurut with the Ogol Lava, separated by a distance of 23 km, suggests they are dynamically related, perhaps through a direct magmatic connection or indirectly via synchronized volcanism. The narrow age grouping of 2.34–2.33 Ma and low-K compositional data illustrated in Figure 9 suggest that the Olgol Lavas, Naisuri Gorge tuffs, and the Lemagurut summit lava were all generated from the same magmatic system, namely Lemagurut Volcano. Zaitsev et al. (2021) explored the link between the Ogol lavas and Lemagurut using petrologic and isotopic data and favored a model involving multiple stages of magma mixing and mingling between the two, which potentially both derived from the same original basaltic melt mantle sources.

https://doi.org/10.1017/qua.2025.17 Published online by Cambridge University Press

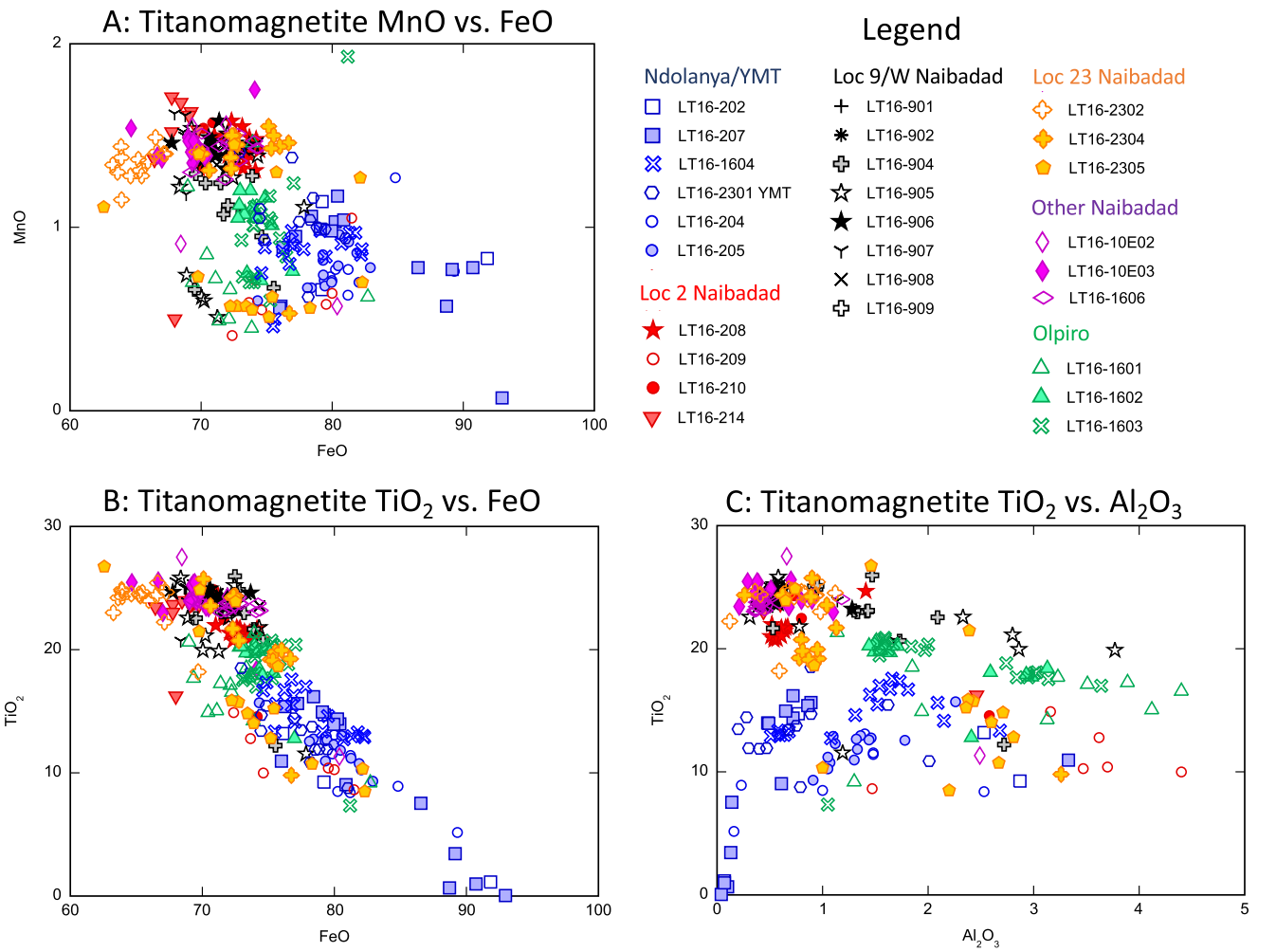

Figure 13. Electron probe microanalysis (EPMA) of titanomagnetite compositions. (A) MnO versus FeO. This plot shows the higher Fe and lower Mn composition of the Ndolanya Beds titanomagnetite (blue symbols) and reveals likely detrital contamination of Ndolanya Beds-derived titanomagnetite into specific Naibadad Beds tuffs (e.g., LT16-23.05). Olpiro tuffs (green symbols) are intermediate. (B) TiO_2 versus FeO shows a similar separation between Naibadad and Ndolanya. (C) TiO_2 versus Al_2O_3. Some of the Ndolanya Beds oxides trend towards magnetite, while Olpiro tuffs trend towards higher Ti and Al.

Major compositional trends

Augite, feldspar, glass, and titanomagnetite compositions for the tuffs analyzed in this study are plotted in Figures 10–13. While the tuffs of the Laetolil, Ndolanya, Naibadad, and Olpiro beds differ significantly from each other in terms of their mineral assemblages, compositions, and ages (see Hay, 1987; McHenry, 2011), compositions within each of these stratigraphic units can be quite similar. Thus, composition permits identification of strata at the level of major stratigraphic units (i.e., attribution of a tuff to the Ndolanya Beds, Lower Naibadad Beds, or Olpiro Beds, but rarely any more stratigraphically specific than that), a powerful capability given the complex erosional, tectonic, and depositional history of the area, but the correlation of individual tuffs between sites is more problematic.

Based on the tephra mineral assemblages for the Laetoli area stratigraphic units documented by Hay (1987) and McHenry (2011) (Figure 2), the Naibadad Beds tuffs are rhyolites with feldspar, augite, and titanomagnetite compositions that distinguish them from both the underlying Ndolanya and overlying Olpiro beds. Overall, their augite is higher in Fe than the Olpiro Tuff and lower in Na than the Ndolanya tuffs (Figure 10). A distinctive low-Na and intermediate- to high-Fe augite population occurs in all Naibadad Beds tuffs sampled, which is not observed in tuffs from the other beds. The Olpiro Tuff is limited to lower-Fe, higher-Ti augite. Ndolanya Beds augite trends towards higher Na and Fe but partially overlaps the Olpiro Tuff at the lower-Fe end of this trend. Many Naibadad Beds tuffs contain populations of higher-Na augite in addition to their distinctive low-Na augite. Naibadad Beds feldspar is dominated by anorthoclase (mostly high-K, Figure 11), unlike the more K-rich sanidine of the Ndolanya tuffs or the intermediate plagioclase of the Olpiro Tuff. The high-Ti and low-Al titanomagnetite compositions of the Naibadad Beds tuffs also separate them from both the Ndolanya Beds and Olpiro Tuff (Figure 13).

An additional key difference between the beds is the abundance of hornblende and plagioclase in the Olpiro Tuff (both are rare to absent in all other units). Andradite (melanite) garnet is abundant in most Ndolanya and Laetolil beds tuffs (although andradite from each of those beds is compositionally distinct; see McHenry, 2011) but absent from the Naibadad and Olpiro beds tuffs (Hay, 1987), except for the basal Naibadad Beds tuff.

https://doi.org/10.1017/qua.2025.17 Published online by Cambridge University Press

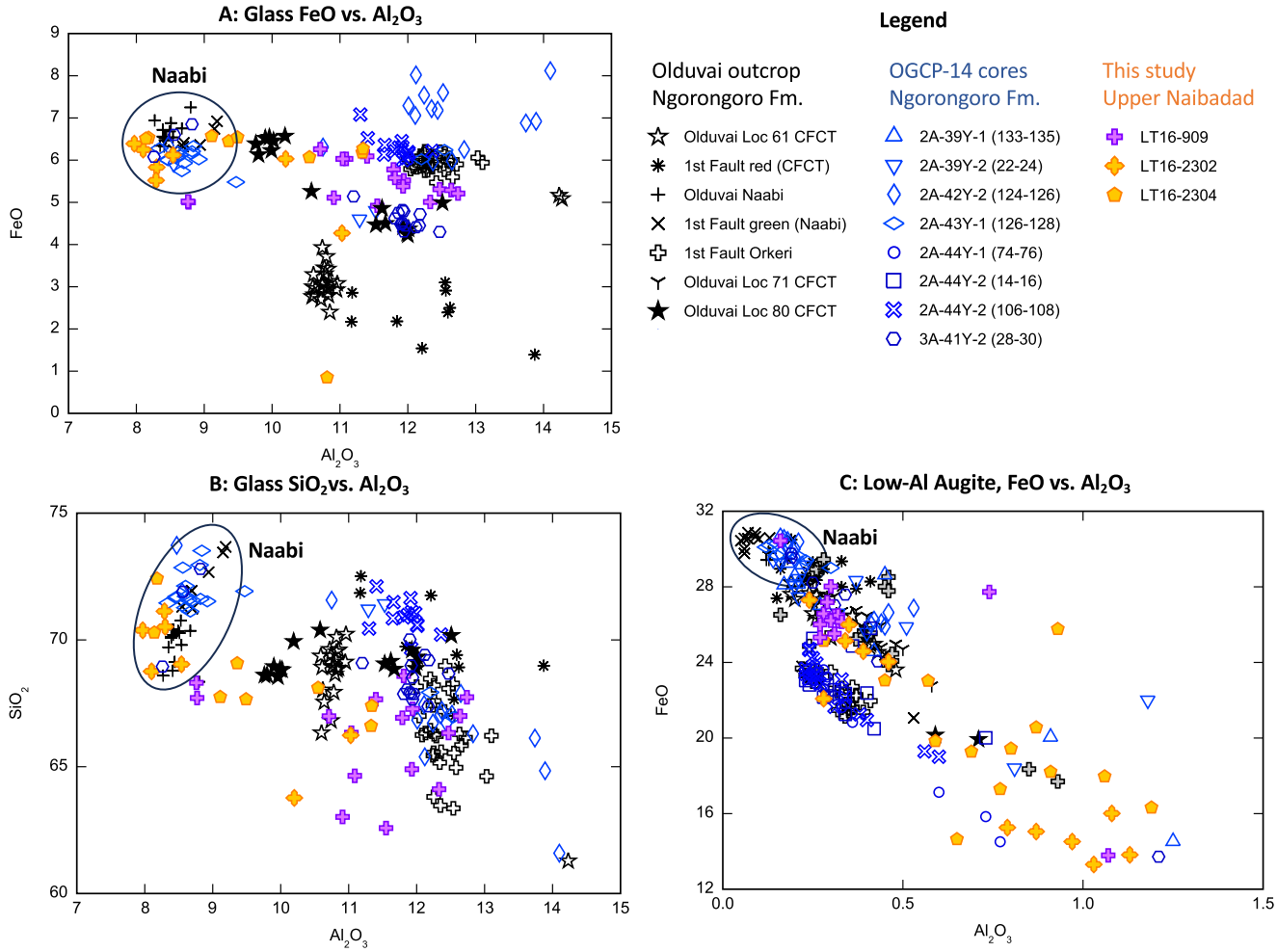

Figure 14. Electron probe microanalysis (EPMA) of glass and augite compositions, compared to Olduvai. Plots include data from three Upper Naibadad samples (orange and purple symbols) from the current study and published EPMA data for Olduvai outcrop tephra (black symbols; McHenry et al., 2008) and OGCP core samples from Cores 2A and 3A (blue symbols; McHenry et al., 2020). (A) FeO versus Al_2O_3 (glass). (B) SiO_2 versus Al_2O_3 (glass). (C) FeO versus Al_2O_3 (augite, low-Al range only). Most glass shards from Naabi Ignimbrite-aged sample LT16-23.02 overlap with the Naabi ignimbrite (outcrop) and Naabi samples from Core 2A. However, as shown in C, the augites of this sample are compositionally unlike the Naabi.

While glass is not preserved in all samples, where present the Naibadad and Olpiro beds tuffs are distinct from each other, with the former characterized by rhyolitic or high-Si trachytic glass and the latter with trachytic to phonolitic glass with higher Al_2O_3 (Figure 12). No Ndolanya samples from the current study preserved glass, but Hay (1987) reported a nepheline phonolite composition.

Distribution of Olpiro Tuff

Except for the type locality for the Olpiro Beds (Locality 16, based on Hay, 1987), we were unable to identify the Olpiro Tuff at any of the locations at which the unit was previously reported (Localities 1, 2N or 2S, or 23). Either no tuff was found in the currently accessible exposures (e.g., Locality 23), or sampled tuffs were mineralogically or chronologically dissimilar (e.g., Localities 1, 2N, and 2S) from the Olpiro Tuff described by Hay (1987) and from our sampling of the tuff at Locality 16.

Hay (1987) described an assemblage of augite, hornblende, and anorthoclase/plagioclase feldspar for the Olpiro Tuff, in which andradite (melanite) garnet is absent. Samples of the Olpiro Tuff from Locality 16 in the current study are consistent with this, with augite higher in Mg than in tuffs from the other beds at Laetoli, abundant hornblende, and mostly plagioclase feldspar. Where glass is present, it is trachytic. However, this assemblage is not observed in samples from the Olpiro Beds elsewhere. In the case of Localities 1 and 2N, candidate Olpiro Beds tuffs were compositionally more like the older Ndolanya Beds, with high-Na augite, andradite garnet, and lack of hornblende.

Possible explanations for this discrepancy

One possibly explanation for this discrepancy is that some deposits previously assigned to the Olpiro Beds could be Ndolanya Beds exposures. The complex depositional, tectonic, and erosional history of the Laetoli area can confuse stratigraphic relationships, and the Ndolanya and Olpiro beds have some similar properties (e.g., both are dark and clay-rich). This is the most likely explanation for Locality 1, where the dark tuff near the top of the "Olpiro" Beds (described in Hay, 1987) clearly matches the Ndolanya Beds in both mineral composition (LT16-1.01) and age (sample L16/1-1). The same is true for a candidate Olpiro Beds exposure at Locality 2N

https://doi.org/10.1017/qua.2025.17 Published online by Cambridge University Press

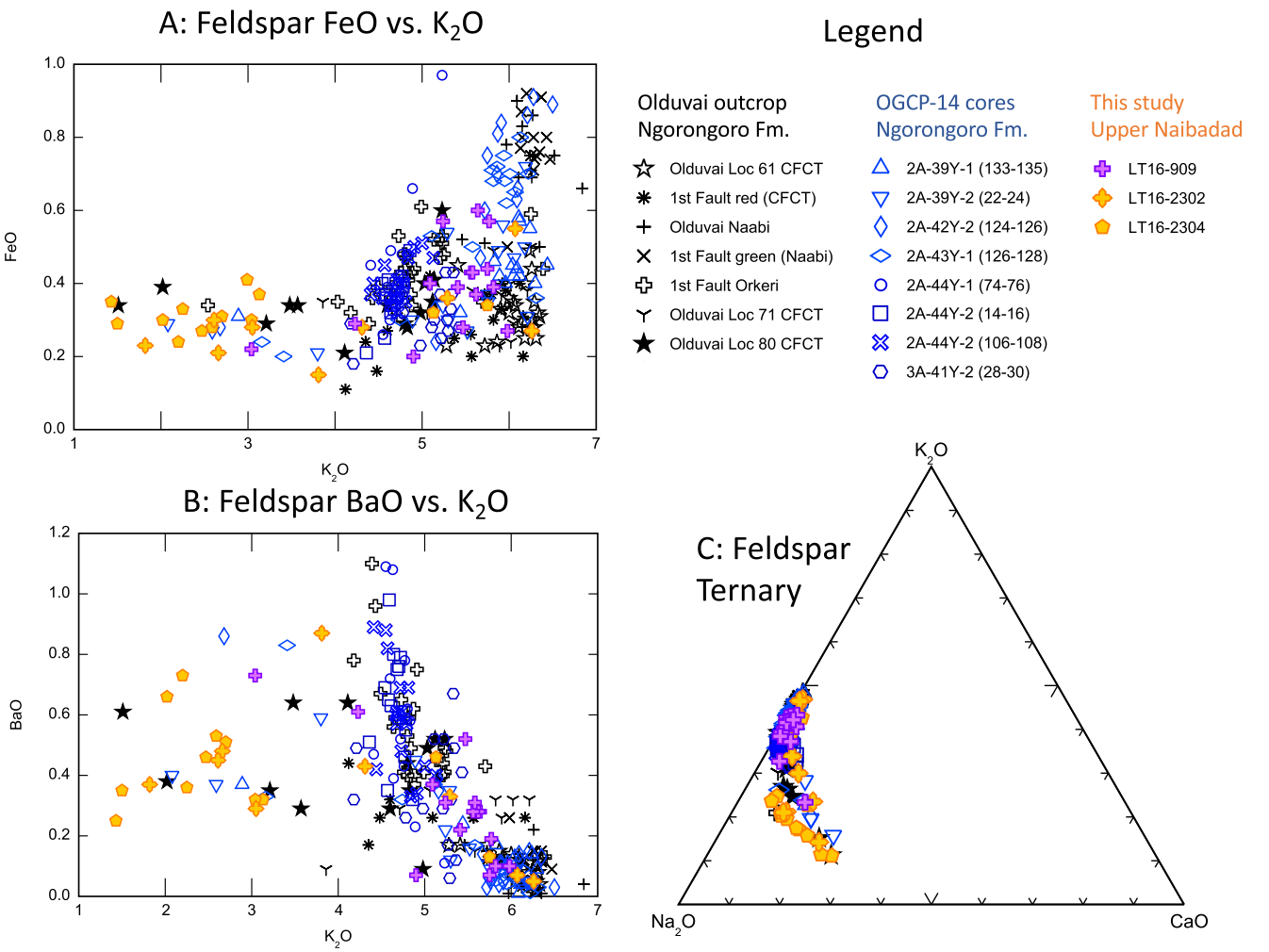

Figure 15. Electron probe microanalysis (EPMA) of feldspar compositions compared to Olduvai. Plots include data from three Upper Naibadad samples (orange and purple symbols) from the current study and published EPMA data for Olduvai outcrop tephra (black symbols; McHenry et al., 2008, 2020) and OGCP core samples from Cores 2A and 3A (blue symbols; McHenry et al., 2020). (A) FeO versus K_2O (feldspar). (B) BaO versus K_2O (feldspar). (C) Feldspar ternary diagram. These plots demonstrate that none of the Naibadad Beds samples contains the distinctive high-Fe anorthoclase composition characteristic of the Naabi Ignimbrite in outcrop or its correlative units in the OGCP cores.

(tuff: LT16-2.05; age: L16/2-1sw), while a second horizon from the same exposure yielded a Naibadad Bed age (L16/2-1w).

A second reason could be confusion in identifying Olpiro Tuff versus upper Naibadad tuffs, without supporting mineral compositional data. This is a possible explanation for the Olpiro Beds at Locality 2S (proposed by Manega, 1993). The tuff indicated in Manega's (1993) stratigraphic section as the Olpiro Tuff is mineralogically consistent with the Naibadad rather than Olpiro beds (sample LT16-2.14: Fe-rich augite, anorthoclase rather than plagioclase, and no hornblende), and yields a Lower Naibadad Beds age (sample L16/2s-4, 2.189 ± 0.004 Ma).

It should be noted that neither of these explanations negates the existence of the Olpiro Beds, as previously described by Hay (1987) and excavated by Ndessokia (1990). The Olpiro Tuff, described here (and by Hay, 1987) for Locality 16, may not be present at all sites corresponding to the Olpiro Beds. It should also be noted that the published age of the Olpiro Tuff (Deino, 2011) places it at ca. 2.057 ± 0.015 Ma, which overlaps the ages obtained for the Upper Naibadad Beds in the current study.

Correlations within Laetoli

While most exposures of the Naibadad Beds contain one or two distinct tuffs, Locality 9/9W exposures include multiple tuffs separated by calcretes indicating gaps in time between deposition. Compositionally, the lowest tuff in the series (geochemical sample LT16-9.04, $^{40}Ar/^{39}Ar$ sample L16/9w-1) includes andradite (melanite) garnet, which is absent or rare in overlying tuffs. This tuff has trachytic glass, with an age of 2.175 ± 0.005 Ma. An andradite and trachytic glass-bearing tuff is also recognized in the lower Naibadad Beds at other sites in the Laetoli area, including Locality 2N (geochemical sample LT16-2.06, $^{40}Ar/^{39}Ar$ sample L16/2-2c: 2.164 ± 0.006 Ma).

Based on their $^{40}Ar/^{39}Ar$ ages, as outlined above, the Naibadad Beds tephra sampled for this study can be divided into three distinct age groups, within which samples mostly overlap within error. However, beyond the distinctive andradite-bearing mineral assemblage observed in the lower tuff described above, few systematic differences in mineral assemblage, mineral composition, or major element glass composition were observed among the different age

https://doi.org/10.1017/qua.2025.17 Published online by Cambridge University Press

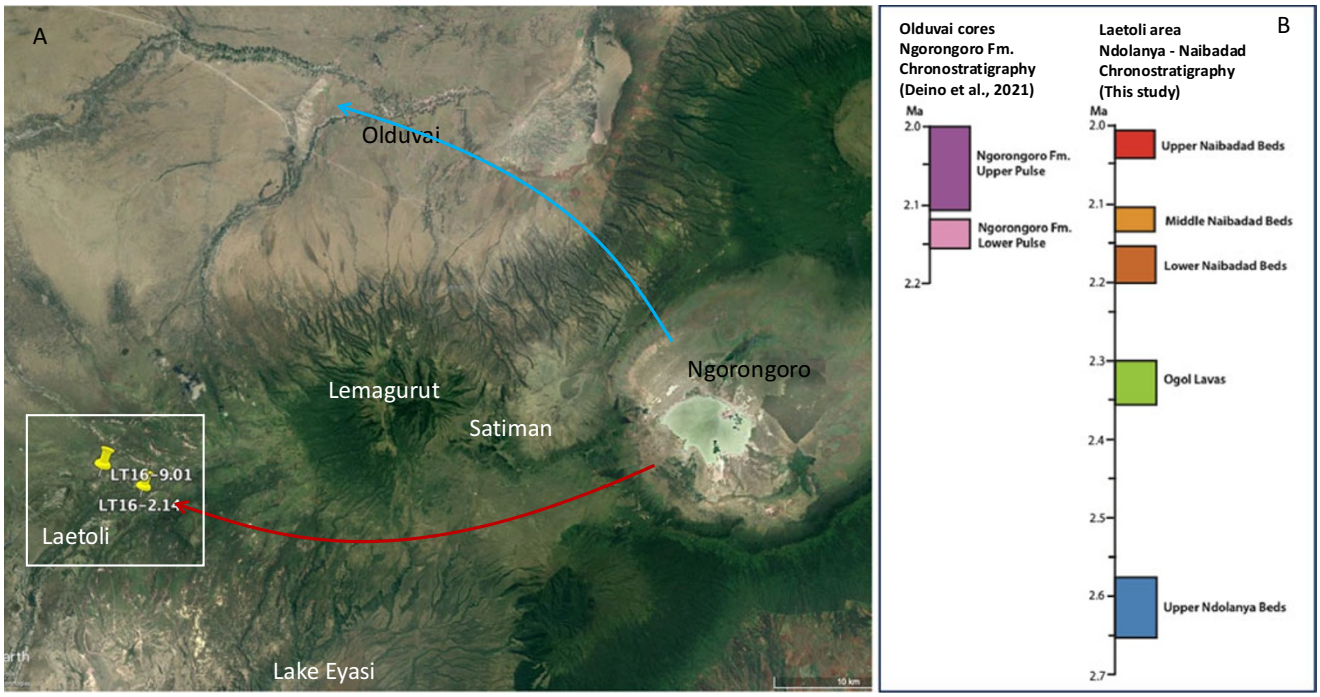

Figure 16. (A) Map showing likely flow directions for Ngorongoro tephra emplacement at Olduvai and Laetoli. Lemagurut and Sadiman volcanoes both pre-date the Naibadad Beds and would have provided an obstacle for the emplacement of Ngorongoro-derived flows from the direction of Olduvai. (B) Chronostratigraphy of the Laetoli area from Upper Ndolanya Beds through the Upper Naibadad Beds, based on the $^{40}Ar/^{39}Ar$ ages reported in this study, compared to the Ngorongoro Formation (Olduvai cores) (after Deino et al., 2021). Bed duration encompasses the range of ages from the oldest- to youngest-dated sample attributed to a chronostratigraphic group in this study, including uncertainties. The Ngorongoro Formation at Olduvai (upper and lower pulses) overlap the age ranges of the Upper and Middle Naibadad Beds at Laetoli.

groups. Some (but not all) of the youngest Naibadad Beds samples, especially LT16-23.02 (equivalent to Ar sample L16/23-2) and LT16-23.04 (top and bottom of the same unit at Locality 23), plot apart from the rest of the Naibadad Beds in FeO in feldspar (lower), Al_2O_3 in augite (lower), and SiO_2 in glass (higher). Both of these samples also contain minor aenigmatite, a mineral absent from all other Laetoli-area tuffs analyzed but present in the Naabi Ignimbrite and related units in the OGCP cores at Olduvai. As noted above, however, we did observe a slight progressive decrease in Ca/K ratio of feldspars analyzed for $^{40}Ar/^{39}Ar$ dating across the three age groups (Figure 9).

Possible correlations to Olduvai

Similarities in composition between the Naibadad Beds and Ngorongoro-derived tuffs, and the lack of other local rhyolitic and trachytic volcanoes of similar age, support a Ngorongoro source for the Naibadad Beds tuffs and tuffaceous material (Deino, 2011; McHenry, 2011). Ngorongoro-derived rhyolites and trachytes are also preserved at Olduvai, at the base of outcrop exposures in Lower Bed I in the western part of Olduvai Gorge (Naabi Ignimbrite, Coarse Feldspar Crystal Tuff (CFCT)), along the 1st fault at the far eastern end of Olduvai (Naabi, CFCT, and Orkeri units; McHenry et al., 2008), and within the OGCP cores (McHenry et al., 2020).

While overall similar in age, assemblage, and composition, no volcanic deposits from Olduvai outcrops or the OGCP cores appear to have exact correlatives to the Naibadad Beds tuffs analyzed in this study. The Naabi Ignimbrite, dated at Olduvai to 2.033 Ma (Deino et al., 2021), has distinctively high-Fe anorthoclase feldspar and Fe-rich augite, along with minor aenigmatite. Similarly aged tuffs in the Naibadad Beds (e.g., samples LT16-23.02, 23.04, and 9.09) have different mineral compositions or assemblages. While minor aenigmatite was identified in both samples LT16-23.02 (Ar sample L16/23-2) and LT16-23.04, and their glass compositions are similar, their feldspar and augite compositions do not overlap with Naabi compositions from Olduvai (Figures 14 and 15). Upper Naibadad Beds sample LT16-9.09 is compositionally similar to the Orkeri Tuff (dated to 2.047 Ma; Deino et al., 2021) in its overall assemblage, but its feldspar has higher K and lower Ba.

Also, many of these units at Olduvai were ignimbrite or volcaniclastic-flow deposits, presumably emplaced directly from Ngorongoro, uphill from Olduvai. At Laetoli, while some Naibadad Beds tuffs are coarse grained (coarse lapilli/pumice bearing), they are direct fallout or fluvially reworked deposits, rather than ignimbrites or flows.

Results from the OGCP cores show that Olduvai was a depocenter prior to and during emplacement of the Naibadad Beds. This is demonstrated by a prominent lacustrine interval at Olduvai situated between two pulses of Ngorongoro volcanic activity (Stanistreet et al., 2020). This activity falls within the timeframe of Naibadad Beds deposition, yet lacustrine strata are not observed at Laetoli. The Olduvai Basin is also at present more than 300 meters topographically lower than Laetoli and, given the absence of known major faults between the OGCP drill sites and Laetoli, this topographic relationship was likely the same during deposition of the Naibadad Beds. The lahars and ignimbrites deposited at Olduvai directly from Ngorongoro volcano would have been prevented from reaching the Laetoli area due to the shielding effect of Lemagurut volcano, which was fully formed by 2.3 Ma

https://doi.org/10.1017/qua.2025.17 Published online by Cambridge University Press

(Figures 9 and 16). These deposits would also largely have been excluded from reaching Laetoli from Olduvai by the requirement of traveling uphill (although not impossible, particularly for pyroclastic flows).

We conclude that the Naibadad Beds tuffs were likely emplaced as fallout directly from Ngorongoro volcano (sometimes locally reworked), rather than having arrived from the Olduvai Basin, and that the Laetoli area was a shielded reentrant in the broader basin paleotopography. Prevailing winds, both now and inferred for the Pleistocene (based on adhesion ripples in a ca. 1.8-Ma tuff at Olduvai; Hay, 1976), are northeasterly to easterly, consistent with transport of volcanic plumes from Ngorongoro in the direction of both Olduvai and Laetoli.

The Naibadad Beds tephra could have instead been emplaced by a tephra cloud following a southern route, traveling from Ngorongoro volcano over the summits of Sadiman and Lemagurut volcanoes or from the southern rim of Ngorongoro volcano around the south sides of these volcanoes and into the Laetoli area. The Eyasi escarpment, which could potentially divert Ngorongoro-derived drainages to the south, most likely post-dates the Naibadad Beds since most of the surface extension of the Eyasi basin occurred within the last 1.5 Ma (Le Gall et al., 2008; Fletcher et al., 2018).

Hay (1987) established that the Naibadad Beds tuffs were deposited in channel fills cut deep into the Ndolanya and Laetolil beds in places, along trends consistent with modern drainages. This implies that the modern southwest-trending drainage was already established by ca. 2.2 Ma. In our model, tephra fallout from Ngorongoro deposited at Laetoli and on the slopes of neighboring volcanoes, and/or volcaniclastic flows exiting the southern rim of Ngorongoro traveling southwest around Sadiman and Lemagurut, were redeposited fluvially as the Naibadad Beds, filling channels previously incised into the Ndolanya and Laetolil beds.

The lack of tephra with the exact same compositions in the Olduvai cores suggests that any tephra fallout cloud was of limited geographical extent, supplying tephra to the south but not the west. This could explain why, while similar, the Ngorongoro-derived tuffs preserved in the Olduvai basin are not the exact same units deposited in the Naibadad Beds at Laetoli. Different eruptions might have followed different paths (west, into Olduvai, or south, into the headwaters of Laetoli drainages). This also explains why some of the Naibadad Beds tuffs are coarse, but do not show surge, flow, or lahar features, why Naibadad Beds tuff deposits are thicker farther away from Lemagurut, and why they often fill incised channels. This could also explain a greater degree of detrital contamination in the Naibadad Beds observed in the mineral assemblages, as they were reworked in drainages containing materials derived from Ndolanya and Laetolil beds.

Implications and conclusions

The Naibadad Beds overlap in time and composition with the Ngorongoro Formation volcaniclastics described in the OGCP cores. The lacustrine interval between the two pulses of Ngorongoro volcanism in OGCP Core 2A occurred during Naibadad times, perhaps during a lull in volcanic activity not preserved at Laetoli.

If Eyasi was not present, the Olduvai basin might have been the local depocenter for the Laetoli area and the most local source of non-spring freshwater—not just during Naibadad Beds times, but earlier. The OGCP cores preserve sediments older than the Naibadad (as old as 2.24 Ma; Deino et al., 2021), and a seismic survey of the Olduvai basin reveals that the basin is substantially deeper and could contain a sedimentary record about twice as thick as was sampled in the 2014 cores (Lu et al., 2019). This older basin fill, not yet cored, could include Ndolanya or even Laetolil beds-aged sediments, as Laetolil Beds-equivalent materials are known to underlie the Olduvai Beds in the southwestern corner of the Olduvai basin (Hay, 1976).

If the Naibadad Beds include eruptive events from Ngorongoro not recorded in the OGCP cores, then they will need to be considered to obtain the complete record of Ngorongoro explosive volcanism (and evolution of the Ngorongoro caldera system). The dates reported here can help constrain this.

Supplementary material. The supplementary material for this article can be found at https://doi.org/10.1017/qua.2025.17

Acknowledgments. The Laetoli field project was funded by the National Geographic Society, Leakey Foundation, and National Science Foundation [BCS-0309513, BCS-1350023, BCS-1322017, and EAR-2020044]. Permits were provided by the Tanzanian Commission for Science and Technology (COSTECH) and the Tanzanian Antiquities Division in Dar es Salaam. This manuscript was greatly improved thanks to feedback from Associate Editor Curtis Marean, reviewer Craig Feibel, and an anonymous reviewer.

References

Arenson, J.L., Harrison, T., Sargis, E.J., Taboada, H., Gilbert, C.C., 2022. A new species of fossil guenon (Cercopithecini, Cercopithecidae) from the Early Pleistocene Lower Ngaloba Beds, Laetoli, Tanzania. *Journal of Human Evolution* **163**, 103136. https://doi.org/10.1016/j.jhevol.2021.103136.

Day, M.H., Leakey, M.D., Magori, C., 1980. A new hominid fossil skull (L.H. 18) from the Ngaloba Beds, Laetoli, northern Tanzania. *Nature* **284**, 55–56.

Deino, A.L., 2011. $^{40}Ar/^{39}Ar$ dating of Laetoli, Tanzania. In: Harrison, T. (Ed.), *Paleontology and Geology of Laetoli: Human Evolution in Context: Volume 1: Geology, Geochronology, Paleoecology and Paleoenvironment*. Springer, Dordrecht, pp. 77–97.

Deino, A.L., 2012. $^{40}Ar/^{39}Ar$ dating of Bed I, Olduvai Gorge, Tanzania, and the chronology of early Pleistocene climate change. *Journal of Human Evolution* **63**, 251–273.

Deino, A.L., Dommain, R., Keller, C.B., Potts, R., Behrensmeyer, A.K., Beverly, E.J., King, J., *et al*, 2019a. Chronostratigraphic model of a high-resolution drill core record of the past million years from the Koora Basin, south Kenya Rift: overcoming the difficulties of variable sedimentation rate and hiatuses. *Quaternary Science Reviews* **215**, 213–231.

Deino, A.L., Sier, M.J., Garello, D.I., Keller, C.B., Kingston, J.D., Scott, J.J., Dupont-Nivet, G., Cohen, A.S., 2019b. Chronostratigraphy of the Baringo–Tugen Hills–Barsemoi (HSPDP-BTB13-1A) core – $^{40}Ar/^{39}Ar$ dating, magnetostratigraphy, tephrostratigraphy, sequence stratigraphy and Bayesian age modeling. *Palaeogeography, Palaeoclimatology, Palaeoecology* **570**, 109519. https://doi.org/10.1016/j.palaeo.2019.109519.

Deino, A.L., Heil, C. Jr, King, J., McHenry, L.J., Stanistreet, I.G., Stollhofen, H., Njau, J.K., Mwankunda, J., Schick, K.D., Toth, N., 2021. Chronostratigraphy and age modeling of Pleistocene drill cores from the Olduvai basin, Tanzania (Olduvai Gorge coring project). *Palaeogeography, Palaeoclimatology, Palaeoecology* **571**, 109990. https://doi.org/10.1016/j.palaeo.2020.109990.

Ditchfield, P., Harrison, T., 2011. Sedimentology, lithostratigraphy and depositional history of the Laetoli area. In: Harrison, T. (Ed), *Paleontology and Geology of Laetoli: Human Evolution in Context: Volume 1: Geology, Geochronology, Paleoecology and Paleoenvironment*. Springer, Dordrecht, pp. 47–76.

Drake, R., Curtis, G.H., 1987. K–Ar geochronology of the Laetoli fossil localities. In: Leakey, M.D., Harris, J.M. (Eds.), *Laetoli: A Pliocene Site in Northern Tanzania*. Clarendon Press, Oxford, pp. 48–52.

Fleck, R.J., Sutter, J.F., Elliot, D.H., 1977. Interpretation of discordant $^{40}Ar/^{39}Ar$ age-spectra of Mesozoic tholeiites from Antarctica. *Geochimica et Cosmochimica Acta* **41**, 15–32.

Fletcher, A.W., Abdelsalam, M.G., Emishaw, L., Atekwana, E.A., Laó-Dávila, D.A., Ismail, A., 2018. Lithospheric controls on the rifting of the Tanzanian craton at the Eyasi basin, eastern branch of the East African rift system. *Tectonics* **37**, 2818–2832.

Harris, J.W.K., Harris, K., 1981. A note on the archaeology at Laetoli. *Nyame Akuma* **18**, 18–21.

Harrison, T. (Ed.), 2011a. *Paleontology and Geology of Laetoli: Human Evolution in Context: Volume 1: Geology, Geochronology, Paleoecology and Paleoenvironment*. Springer, Dordrecht.

Harrison, T., 2011b. *Paleontology and Geology of Laetoli: Human Evolution in Context: Volume 2: Fossil Hominins and the Associated Fauna*. Springer, Dordrecht.

Harrison, T., 2011c. Introduction: the Laetoli hominins and associated fauna. In: Harrison, T. (Ed.), *Paleontology and Geology of Laetoli: Human Evolution in Context: Volume 2: Fossil Hominins and the Associated Fauna*. Springer, Dordrecht, pp. 1–14.

Harrison, T., 2011d. Hominins from the Upper Laetolil and Upper Ndolanya beds, Laetoli. In: Harrison, T. (Ed.), *Paleontology and Geology of Laetoli: Human Evolution in Context: Volume 2: Fossil Hominins and the Associated Fauna*. Springer, Dordrecht, pp. 141–188.

Harrison, T., Kweka, A., 2011. Paleontological localities on the Eyasi Plateau, including Laetoli. In: Harrison, T. (Ed.), *Paleontology and Geology of Laetoli, Tanzania: Human Evolution in Context: Volume 1: Geology, Geochronology, Paleoecology and Paleoenvironment*. Springer, Dordrecht, pp. 17–45.

Harrison, T., Kwekason, A., Su, D., 2022. Paleoecology of Laetoli, Tanzania. In: Reynolds, S.C., Bobe, R. (Eds.), *African Paleoecology and Human Evolution*. Cambridge University Press, Cambridge, UK, pp. 435–452.

Hay, R.L., 1976. *Geology of the Olduvai Gorge: A Study of Sedimentation in a Semiarid Basin*. University of California Press, Berkeley, 203 pp.

Hay, R.L., 1987. Geology of the Laetoli area. In: M.D. Leakey, J.M. Harris (Eds.), *Laetoli, A Pliocene Site in Northern Tanzania*. Oxford University Press, New York, 561 pp.

IUGS, **Le Maitre, R.W.**, 1989. *A Classification of Igneous Rocks and Glossary of Terms: Recommendations of the International Union of Geological Sciences Subcommission on the Systematics of Igneous Rocks*. Blackwell, Oxford.

Keller, C.B., 2018. Chron.jl: a Bayesian framework for integrated eruption age and age-depth modelling. https://doi.org/10.17605/OSF.IO/TQX3F.

Le Gall, B., Nonnotte, P., Rolet, J., Benoit, M., Guillou, H., Mousseau-Nonnotte, M., Albaric, J., Déverchère, J., 2008. Rift propagation at craton margin.: Distribution of faulting and volcanism in the North Tanzanian Divergence (East Africa) during Neogene times. *Tectonophysics* **448**, 1–19.

Leakey, M.D., 1987a. The hominid footprints: introduction. In: Leakey, M.D., Harris, J.M. (Eds.), *Laetoli: A Pliocene Site in Northern Tanzania*. Clarendon Press, Oxford, pp. 490–496.

Leakey, M.D., 1987b. The Laetoli hominid remains. In: Leakey, M.D., Harris, J.M. (Eds.), *Laetoli: A Pliocene Site in Northern Tanzania*. Clarendon Press, Oxford, pp. 108–117.

Leakey, M.D., 1987c. introduction. In: Leakey, M.D., Harris, J.M. (Eds.), *Laetoli: A Pliocene Site in Northern Tanzania*. Clarendon Press, Oxford, pp. 1–22.

Leakey, M.D., Harris, J.M. (Eds.), 1987. *Laetoli: A Pliocene Site in Northern Tanzania*. Clarendon Press, Oxford.

Lee, J.Y., Marti, K., Severinghaus, J.P., Kawamura, K., Yoo, H.S., Lee, J.B., Kim, J.S., 2006. A redetermination of the isotopic abundances of atmospheric Ar. *Geochimica et Cosmochimica Acta* **70**, 4507–4512.

Lu, K., Hanafy, S., Stanistreet, I., Njau, J., Schick, K., Toth, N., Stollhofen, H., Schuster, G., 2019. Seismic imaging of the Olduvai basin, Tanzania. *Palaeogeography, Palaeoclimatology, Palaeoecology* **533**, 109246. https://doi.org/10.1016/j.palaeo.2019.109246.

Manega, P.C., 1993. Geochronology, geochemistry and isotopic study of the Plio-Pleistocene hominid sites and the Ngorongoro volcanic highland in northern Tanzania. [PhD dissertation] University of Colorado, Boulder.

Masao, F.T., Kimambo, J.S., 2021. Further notes on the Ngaloba industry, a Middle Stone Age assemblage directly associated with early *Homo* in the greater Laetoli, Northern Tanzania. In: Fortes-Lima, C., Mtetwa, E., Schlebusch, C. (Eds.), *Africa, the Cradle of Human Diversity: Cultural and Biological Approaches to Uncover African Diversity*. Brill, Leiden, pp. 43–60.

Masao, F.T., Ichumbaki, E.B., Cherin, M., Barili, A., Boschian, G., Iurino, D.A., Menconero, S., Moggi-Cecchi, J., Manzi, G., 2016. New footprints from Laetoli (Tanzania) provide evidence for marked body size variation in early hominins. *eLife 2016* **5**, e19568. https://doi.org/10.7554/eLife.19568.

McDougall, I., Harrison, T.M., 1999. *Geochronology and Thermochronology by the $^{40}Ar/^{39}Ar$ Method*, 2nd ed. Oxford University Press, Oxford, 269 pp.

McHenry, L.J., 2011. Geochemistry and mineralogy of Laetoli area tuffs: lower Laetolil through Naibadad Beds. In T. Harrison (Ed.), *Paleontology and Geology of Laetoli, Tanzania: Human Evolution in Context: Volume 1: Geology, Geochronology, Paleoecology and Paleoenvironment*. Springer, Dordrecht, pp. 121–141.

McHenry, L.J., Mollel, G.F., Swisher, C.C., 2008. Compositional and textural correlations between Olduvai Gorge Bed I tephra and volcanic sources in the Ngorongoro volcanic highlands, Tanzania. *Quaternary International* **178**, 306–319.

McHenry, L.J., Njau, J.K., de la Torre, I., Pante, M.C., 2016. Geochemical "fingerprints" for Olduvai Gorge Bed II tuffs and implications for the Oldowan–Acheulean transition. *Quaternary Research* **85**, 147–158.

McHenry, L.J., Stanistreet, I.G., Stollhofen, H., Njau, J.K., Toth, N., Schick, K., 2020. Tuff fingerprinting and correlations between OGCP cores and outcrops for Pre-Bed I and Beds I/II at Olduvai Gorge, Tanzania. *Palaeogeography, Palaeoclimatology, Palaeoecology* **548**, 109630. https://doi.org/10.1016/j.palaeo.2020.109630.

Min, K., Mundil, R., Renne, P.R., Ludwig, K.R., 2000. A test for systematic errors in $^{40}Ar/^{39}Ar$ geochronology through comparison with U/Pb analysis of a 1.1-Ga rhyolite. *Geochimica et Cosmochimica Acta* **64**, 73–98.

Mollel, G.F., Swisher, C.C. III, Feigenson, M.D., Carr, J.D., 2011. Petrology, geochemistry and age of Satiman, Lemagurut and Oldeani: sources of the volcanic deposits of the Laetoli area. In: Harrison, T. (Ed.), *Paleontology and Geology of Laetoli, Tanzania: Human Evolution in Context: Volume 1: Geology, Geochronology, Paleoecology and Paleoenvironment*. Springer, Dordrecht, pp. 99–119.

Ndessokia, P.N.S., 1990. The mammalian fauna and archaeology of the Ndolanya and Olpiro Beds, Laetoli, Tanzania. [Ph.D. dissertation] University of California, Berkeley.

Niespolo, E.M., Rutte, D., Deino, A.L., Renne, P.R., 2017. Intercalibration and age of the Alder Creek sanidine $^{40}Ar/^{39}Ar$ standard. *Quaternary Geochronology* **39**, 205–213.

Njau, J.K., Toth, N., Schick, K., Stanistreet, I.G., McHenry, L.J., Stollhofen, H., 2021. The Olduvai Gorge Coring Project: drilling high resolution palaeoclimatic and palaeoenvironmental archives to constrain hominin evolution. *Palaeogeography, Palaeoclimatology, Palaeoecology* **561**, 110059. https://doi.org/10.1016/j.palaeo.2020.110059.

Stanistreet, I.G., Stollhofen, H., Deino, A.L., McHenry, L.J., Toth, N.P., Schick, K.D., Njau, J.K., 2020. New Olduvai Basin stratigraphy and stratigraphic concepts revealed by OGCP cores into the Palaeolake Olduvai depocentre, Tanzania. *Palaeogeography, Palaeoclimatology, Palaeoecology* **554**, 109751. https://doi.org/10.1016/j.palaeo.2020.109751.

Zaitsev, A.N., Arzamastsev, A.A., Marks, M.A., Braunger, S., Wenzel, T., Spratt, J., Salge, T., Markl, G., 2021. Hybridization of alkali basaltic magmas: a case study of the Ogol lavas from the Laetoli area, Crater Highlands (Tanzania). *Journal of Petrology* **62**, egab035. https://doi.org/10.1093/petrology/egab035.

https://doi.org/10.1017/qua.2025.17 Published online by Cambridge University Press